REVIEW

Check for updates

Recent advances in the interfacial engineering of organic–inorganic hybrid perovskite solar cells: a materials perspective

Zhaochen Guo,[a] Zhongbin Wu, [iD][a] Yonghua Chen, [iD][b] Songcan Wang [iD]*[a] and Wei Huang*[a]

Research on perovskites, a highly promising type of semiconductor material in the field of photovoltaics, has made amazing progress. The development of perovskite solar cells (PSCs) has so far reached a certified power conversion efficiency (PCE) of 25.7%. Since the interfaces in PSCs are closely connected to the carrier dynamics (charge separation, transport, injection, collection and recombination), interfacial engineering has become a powerful tool in enhancing the device performance and long-term stability. This review focuses on critically discussing the emerging materials and strategies for interfacial engineering at the charge transport layer (CTL)/perovskite and CTL/electrode interfaces in PSCs with both normal and inverted structures. In particular, the underlying mechanisms of various materials for interfacial engineering in maximizing the PCE and the long-term stability of PSCs are systematically demonstrated. Finally, a brief summary of the latest advances and breakthroughs, and a perspective on the future research directions are presented, which are expected to promote the development of this important research field.

[a] *Frontiers Science Center for Flexible Electronics, Xi'an Institute of Flexible Electronics (IFE), Xi'an Institute of Biomedical Materials & Engineering, Northwestern Polytechnical University, 127 West Youyi Road, Xi'an 710072, China. E-mail: iamscwang@nwpu.edu.cn, iamwhuang@nwpu.edu.cn*
[b] *Key Laboratory of Flexible Electronics (KLOFE) & Institution of Advanced Materials (IAM), Nanjing Tech University (NanjingTech), Nanjing, 211816, China*

1. Introduction

As the global population grows as well as the increasing demand for energy, fossil fuels will gradually face depletion, leading to a non-negligible issue of an energy crisis.[1] On the other hand, the requirement to reduce carbon dioxide emissions has been raised due to the increasing greenhouse effect that has been changing the global climate.[2,3] On Earth, solar energy is extensively distributed and inexhaustible as a

Zhaochen Guo is currently a PhD candidate at the Institute of Flexible Electronics (IFE), Northwestern Polytechnical University (NPU), China, under the supervision of Prof. Songcan Wang. He received his MEng degree in 2021 from the School of Chemistry and Chemical Engineering, Northwestern Polytechnical University. His current research focuses on efficient and stable perovskite photovoltaic devices, including perovskite solar cells as well as perovskite photodetectors.

Zhaochen Guo

Zhongbin Wu obtained his PhD degree from the Chinese Academy of Sciences. He then worked as a Humboldt postdoctoral fellow at TU Dresden. After that, he moved to the University of Toronto to continue his postdoctoral research. Now he is a full professor at Northwestern Polytechnical University, China. His research interests are organic optoelectronic materials and devices, including organic light-emitting diodes, organic thin-film transistors, and organic light-emitting transistors.

Zhongbin Wu

This journal is © The Royal Society of Chemistry 2022

J. Mater. Chem. C, 2022, **10**, 13611–13645 | **13611**

renewable and clean energy source.[4,5] The rational use of solar energy to change the current energy mix has been proved to be one of the most effective methods.[6]

With the rapid development of photovoltaic technology, solar energy can be directly converted into electricity to meet the world's energy needs with little environmental effects.[7] Currently, solar cells are divided mainly into silicon-based solar cells,[8,9] thin-film solar cells,[10] and new solar cells from a developmental stage.[11,12] Compared with traditional solar cells, new solar cells have the advantages of using a simpler preparation process, having cheaper material costs, being more environmentally friendly, and having considerable efficiency, which signifies their huge development potential.

Organic–inorganic hybrid perovskite solar cells (PSCs) are one of the most important new solar cells that have attracted great attention since their first discovery in 2009.[13] The standard formula of the organic–inorganic hybrid perovskite material is ABX_3, where A is an organic cation, such as $CH_3NH_3^+$ (MA^+), $CH(NH_2)_2^+$ (FA^+), $etc.$, B is a metal cation, such as Pb^{2+}, Sn^{2+}, $etc.$, and X is a halogen anion, like Cl^-, Br^-, I^-, $etc.$[14] This material is an excellent light-absorbing material that has a special crystal structure and excellent photoelectric properties, including a long carrier lifetime, a large light-absorption coefficient, a high defect-state tolerance, and a high dielectric constant.[15] In addition, its simple preparation method, low cost, and compatibility with flexible substrates meet the future development needs for flexible or foldable solar cells; hence, its application to new solar cells shows enormous development potential.[16–19] It should be mentioned that the perovskite material was first applied in 2009 as a sensitizer for dye-sensitized solar cells, and obtained a power conversion efficiency (PCE) of only 3.8%, opening up a new era for solar cells.[13] In 2012, a new technique using solid organic–inorganic hybrid perovskites was developed after abandoning the liquid-phase conditions,[20] resulting in a further breakthrough in the photovoltaic performance. Since then, the speed of research related to PSCs has increased. As of 2021, the PCE of PSCs has reached 25.7%.[21]

Despite the outstanding photovoltaic performance of PSCs, their stability and lifetime issues are major challenges for their practical application, and even for their gradual replacement of silicon cells in the future.[22–24] With the rapid development of PSC technology and the maturation of device-preparation processes, the ability to improve their performance indices by improving the device structure has gradually decreased. Therefore, this necessitates a more in-depth investigation of the interfaces between the device layers and the perovskite material itself during the device design and preparation, as well as optimization to obtain better interfacial properties for achieving devices with a higher photovoltaic performance.[25–27] As shown in Fig. 1a, since the photogenerated electron and hole carriers from the perovskite layer will transfer to the electrodes through the charge transport layers (CTLs), the perovskite/CTL and CTL/electrode interfaces are closely connected to the carrier dynamics (*i.e.*, charge separation, transport, injection, collection and recombination) and significantly affect the device performance. Their interfacial defects, interfacial reactions, and nonradiative recombination due to energy-level mismatch have a substantial impact on the performance of the device.[28,29] Interfacial engineering is a means of improving the device performance by adding or changing both the materials and structure of the interface, which can optimize the energy-level alignment, improve the film quality, passivate defects, and enhance the device stability (Fig. 1b). Therefore, interfacial engineering has become an important strategy for enhancing the performance of PSCs.

In recent years, there have been some excellent reviews on interfacial engineering, but most of them have focused only on normal-structured PSCs.[30–32] Owing to the dynamic development of this important research field, a comprehensive review that focuses on the interfacial engineering of PSCs with both

Songcan Wang is currently a professor at the Institute of Flexible Electronics (IFE), Northwestern Polytechnical University (NPU), China. He received his BEng (2011) and MEng (2014) from Central South University (CSU), China, and his PhD degree in 2018 from the University of Queensland (UQ), Australia. Before joining NPU, he worked as a postdoctoral research fellow in Professor Lianzhou Wang's group at UQ for about 1.5 years.

Songcan Wang

His research interests focus on the synthesis of semiconductor nanomaterials for solar energy conversion and storage, including photoelectrochemical cells, photocatalysis, solar cells, and rechargeable batteries.

Wei Huang received his BSc, MSc, and PhD degrees in chemistry from Peking University in 1983, 1988, and 1992, respectively. He was appointed as the Deputy President of Nanjing University of Posts and Telecommunications in 2006, the President of Nanjing Tech University in 2012, and the Provost of Northwestern Polytechnical University in 2017. He is a member of the Chinese Academy of Sciences, Foreign Academician and Honorary Doctor of the Russian

Wei Huang

Academy of Sciences, and Fellow of the Royal Society of Chemistry. His research interests include organic optoelectronics, nanomaterials, polymer chemistry, plastic electronics, and bioelectronics.

Fig. 1 (a) Charge transport diagram of a typical n–i–p PSC. (b) Functions of interfacial engineering in PSCs.

normal and inverted structures remains necessary to provide readers with a better understanding of the state-of-the-art progress in this hot and dynamic research field. Here, recent advances in the modification of different interfaces to improve the performance and stability of PSCs are comprehensively reviewed from the perspective of the materials, which are classified as inorganic salts, organic molecules and polymers, quantum dots (QDs), fullerenes and their derivatives, self-assembled small molecules (SAMs) and two-dimensional (2D) materials. It is worth mentioning that 2D materials include the general 2D materials as well as 2D perovskites. As a typical 2D material, graphene was successfully prepared via a mechanical exfoliation method, initiating the research into 2D materials.[33,34] Graphene has attracted much attention due to its excellent physical properties, which include a high carrier mobility, high

strength, high flexibility and high optical transparency. Fig. 2a represents the graphene crystal structure. Along with graphene, many other 2D materials have been developed. In the research field of PSCs, 2D materials that include graphene and its derivatives as well as transition metal carbides/nitrides (MXenes) are generally applied as interfacial modification materials (Fig. 2b). In addition to being used as light-absorbing layers, 2D perovskites are often used as interfacial modification layers, with the effect of improving the interlayer energy levels, reducing charge recombination, and effectively inhibiting ion migration (Fig. 2c). In this review article, we primarily discuss the up-dated progress that has been reported over the past few years for interfacial engineering at the electron transport layer (ETL)/perovskite, perovskite/hole transport layer (HTL), and CTL/electrode interfaces for PSCs with both normal and inverted structures.

Fig. 2 Crystal structure diagrams for (a) graphene, (b) MXene and (c) 2D perovskite.

This journal is © The Royal Society of Chemistry 2022

J. Mater. Chem. C, 2022, **10**, 13611–13645 | **13613**

This is because these interfaces are the focus of investigations on interface modification and are directly related to the extraction of photogenerated carriers from the perovskite layer. In particular, the strategies of dual interfacial modification, *i.e.*, the simultaneous modification at different interfacial layers, are also critically discussed. Finally, a brief summary of the current research status is presented, along with the prospects of interfacial engineering for the development of efficient, large-area PSCs for possible commercialization.

2. Roles of interfacial engineering

Depending on whether or not the cell structure contains a titanium dioxide (TiO$_2$) mesoporous layer, PSCs can be classified into mesoporous structures and planar heterogeneous structures.[35,36] Thus far, most high-efficiency PSCs are processed with mesoporous TiO$_2$ materials at high temperatures (>450 °C), which is not favorable for the development of low-cost and flexible PSCs. By contrast, planar structures not only simplify the device processing but also enable low-temperature processing, while providing the possibility of preparing stacked devices, which can now achieve device efficiencies close to those of mesoporous structures processed at high temperatures. Fig. 3 shows the schematic diagrams of PSCs with different structures, where planar heterostructure solar cells are subdivided into normal (n–i–p) and inverted (p–i–n) configurations according to the direction of photogenerated carrier transport. More specifically, the mesoporous structure shown in Fig. 3a consists of a transparent conducting oxide cathode (FTO/ITO), a dense ETL (TiO$_2$), a perovskite material attached to a mesoporous metal oxide layer (TiO$_2$ or Al$_2$O$_3$), followed by an HTL as well as a metal electrode. This structure is characterized by its ability to enhance charge accumulation by reducing the carrier diffusion length and also effectively reducing carrier recombination. However, the grain confinement of the perovskite in the mesopores enables a large amount of perovskite to be present in the amorphous phase, resulting in lower short-circuit current (J_{sc}) and open-circuit voltage (V_{oc}) values. In addition, a perovskite with long-lived carriers and long diffusion distances means that it can work even without a mesoporous TiO$_2$ layer, and thus planar structured PSCs emerge.[37,38] Fig. 3b shows the planar n–i–p structure, where the mesoporous layer is omitted and the perovskite layer is sandwiched between the HTL and the ETL.

Compared with mesoporous n–i–p PSCs fabricated using similar materials and methods, the planar n–i–p structure still shows severe *J–V* hysteresis, despite the fact that it yields a higher J_{sc} and V_{oc}.[39] The inverted p–i–n structure is the opposite of the n–i–p structure in the order of light, *i.e.*, ITO/FTO, HTL, perovskite, ETL, metal electrode (Al or Au), as shown in Fig. 3c. With the further development of the p–i–n structure, its ETL and HTL have been extended from specific organic substances to inorganic substances.[40,41]

The interface of PSCs has a profound effect on their photovoltaic performance and lifetime. Firstly, the photovoltaic performance-related parameters such as V_{oc}, J_{sc}, fill factor (FF) and PCE are influenced by the charge extraction and transport between the CTL and the active layer of the perovskite.

The photocurrent density of PSCs is defined from the monochromatic incident photon-to-electron conversion efficiency (IPCE), as illustrated by the following equation:[42]

$$\text{IPCE}(\lambda) = \alpha(\lambda)\varphi_{inj}\varphi_c \tag{1}$$

where α is the absorption rate, φ_{inj} is the charge injection efficiency, and φ_c refers to the charge collection efficiency. Therefore, how to optimize the charge injection and collection efficiencies at the interface with a constant absorption rate determines the final photocurrent density of the device.

Alternatively, the charge injection efficiency is expressed using the following equation:[29]

$$\varphi_{inj} = k_{inj}/(k_{inj} + k_r + k_{nr}) \tag{2}$$

where k_{inj} is the injection rate constant, k_r is the radiative recombination rate, and k_{nr} is the non-radiative recombination rate. To obtain a higher charge injection efficiency φ_{inj}, it is necessary to increase k_{inj} and decrease k_r and k_{nr} as much as possible. The contact between the active layer and the material, and its associated energy level, affect k_{inj}. The choice of material and the quality of the interface affect k_r and k_{nr}. In perovskite materials, the effect of k_r on φ_{inj} is much lower than that of k_{nr}, so improving the interface quality to limit non-radiative recombination at the interface is critical for increasing the photocurrent density of PSCs.[43,44]

Moreover, the non-radiative recombination also has an important effect on the steady-state carrier density, which determines the quasi-Fermi energy level splitting in the device
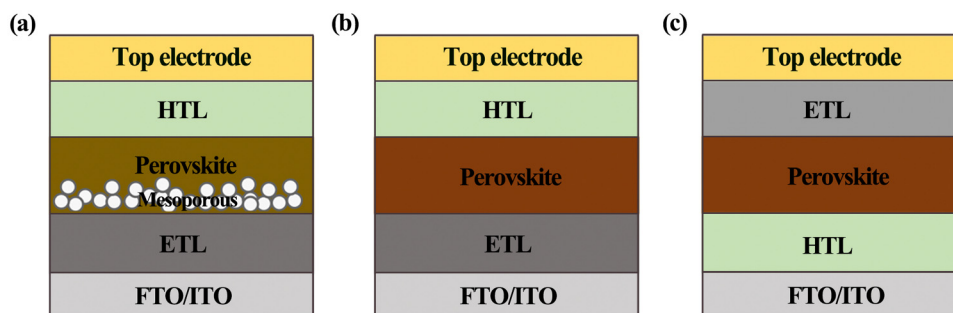

Fig. 3 PSCs with the (a) n–i–p mesoporous structure, (b) n–i–p planar structure, and (c) p–i–n planar structure.

concerning the V_{oc},[45] as is shown by the following equation:[30]

$$V_{oc} = \frac{kT}{q}\ln\left(\frac{J_{ph}}{J_0} + 1\right) \quad (3)$$

where q refers to the charge, k refers to the Boltzmann constant, T refers to the temperature, J_0 refers to the saturation current density, and J_{ph} refers to the photocurrent density. From the equation, it is clear that the energy level arrangement and the interface defect density will be influenced by the interface material, both of which are essential factors in improving the performance of PSCs.[46,47] Moreover, the current–voltage hysteresis and stability are also influenced by the charge transfer at the interfaces.

Furthermore, organic materials (0.1 eV and 10 nm, respectively) have a lower exciton binding energy (30–76 meV) and a longer exciton diffusion length (100–1000 nm), making them easier for excitons and free carriers to diffuse to the interface. Non-radiative energy transfer or exciton dissociation between the layers in PSCs can lead to quenching, which affects the device performance.[48]

In the interfacial engineering of PSCs, the electrode is also an indispensable component, which not only conducts the charge generated by the photovoltaic device to the external circuit to complete the whole photoelectric conversion process, but also affects the quality of the interface layer, the transparency of the photovoltaic device, and the cost of the photovoltaic device preparation. In the preparation of photovoltaic devices, electrodes are an essential and important part. The electrons and holes generated in the device need to reach the top and bottom electrodes through the ETL and HTL, respectively, and finally be collected through the closed external circuit that forms the photocurrents.

For the bottom electrode in the structure of the cells, its morphology and properties have an important influence on the wettability and film quality of the upper interfaces, so the modification of its surface is very important for improving the performance of PSCs. Currently, the most commonly used metal oxide transparent conductive films for the bottom electrode of PSCs are indium-doped tin oxide (ITO) and fluorine-doped tin oxide (FTO), *etc.*, whose photovoltaic properties are closely related to the film thickness and film quality.[49,50] Among them, ITO is commonly used as the bottom electrode for planar structured PSCs. Compared with ITO, FTO has a lower light transmission rate due to its larger thickness, but it is more suitable as a substrate for interfacial layers that require high-temperature heating, such as TiO_2, due to its corrosion resistance and high-temperature tolerance, and is therefore widely used as the bottom electrode for mesoporous structured PSCs. The top electrode plays a crucial role in charge collection in PSCs, and common top electrodes in PSCs are Ag, Al and Au. However, due to their high cost and the degradation of PSCs caused by Ag electrodes in contact with perovskite for a long time, carbon electrodes, transparent conductive metal oxide electrodes, and polymer electrodes are being developed and utilized in addition to metal electrodes.[31,51] In particular, carbon has many advantages such as being an abundant resource, and having a low cost, good conductivity, and good chemical stability. Moreover, its work function (5.0 eV) is similar to that of Au (5.1 eV), which makes carbon an ideal choice for the top electrode of PSCs. In addition, since carbon electrode-based PSCs may not require an HTL, the preparation of HTL-free carbon-based PSCs (C-PSCs) with a lower energy consumption and simpler operation has become a hot research topic in the field of PSCs.[52] In addition, a tight ohmic contact between the electrode and the interface should be achieved to reduce the contact potential barrier at the device interface and obtain a higher PCE.[53]

In particular, semitransparent PSCs (ST-PSCs), with their unique transparent electrode design, can absorb light from both sides and produce a greater energy output compared with single-sided PSCs. Furthermore, ST-PSCs can be stacked with other cells to make full use of the sunlight, and thus have received a lot of attention. At present, the process of silicon-based cells in high-efficiency four-terminal tandem devices has matured, and the cell performance of tandem modules is mainly determined by the upper layer of ST-PSCs.[54,55] Modification of the interface between the electrode and the CTL in ST-PSCs, to make the energy bands more compatible and the charge transfer smoother, will make the preparation of stacked cells more favorable. According to the above analysis, interfacial engineering has been developed as an important tool to accomplish these purposes.

3. Interfacial engineering in the normal structure

3.1 Bottom electrode/perovskite interface

Unlike the top electrode, which needs to be deposited on a fragile and complex perovskite layer or an organic CTL, the bottom electrode can generally be sufficiently stable when combined with a suitable charge transport intermediate layer. In ETL-free PSCs, the majority of work focused on the interfacial modification is devoted to correcting the mismatch in energy levels at the electrode/perovskite interface. A polar non-conjugated small molecule, 4,4-(((methyl(4-sulphonatobutyl)-ammonio)bis(propane-3,1-diyl))bis(dimethyl ammoniumdiyl))-bis-(butane-1-sulfonate) (MSAPBS) was designed as a modifier to reduce the work function of ITO and improve the energy level alignment at the interface through an intrinsic dipole. The electron extraction efficiency was thus greatly improved, followed by significant enhancement of the V_{oc}, J_{sc} and FF of the device. Ultimately, the champion device achieved a PCE of 20.55% (Fig. 4a and b). Simultaneously, its stability was improved.[56] In a similar work, rubidium fluoride (RbF) was inserted on the FTO surface as a modification layer. The RbF layer created a dipole layer, which adjusted the work function of the FTO, eliminated the electron transfer potential barrier, and optimized the energy level arrangement of the FTO/perovskite interface. Consequently, charges were transferred more efficiently and charge-carrier recombination was suppressed. As a result, the efficiency of ETL-free PSCs with the RbF layer reached as high as 18.79% (Fig. 4c and d).[57]
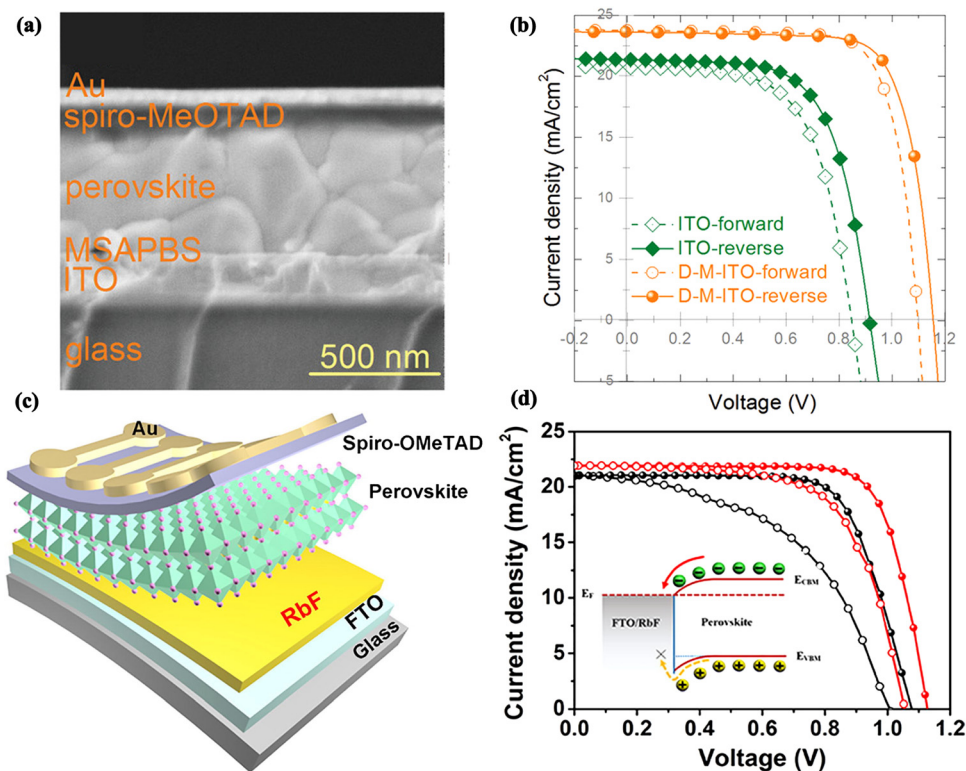
This journal is © The Royal Society of Chemistry 2022

J. Mater. Chem. C, 2022, **10**, 13611–13645 | **13615**

Fig. 4 (a) Cross-sectional SEM image and (b) J−V curves of PSCs for the bottom electrode/perovskite interface of normal structural PSCs based on MSAPBS. Reproduced with permission from ref. 56. Copyright 2020 Wiley. (c) Device structure diagram and (d) J−V curves of PSCs for the bottom electrode/perovskite interface of normal structural PSCs based on RbF. Reproduced with permission from ref. 57. Copyright 2020 Elsevier.

3.2 ETL/perovskite interface

As one of the key interfaces in PSCs, energy-level matching between the ETL and the perovskite layer is crucial for improving the carrier extraction and collection efficiency, as well as the V_{oc} of the device. Too large a difference between the ETL and perovskite layer energy bands will lead to inefficient electron injection into the ETL and V_{oc} reduction. However, a small energy band difference between the ETL and the perovskite layer will also cause ineffective separation of the photogenerated electrons and holes, resulting in significant recombination of the electron–hole pairs.[58] Commonly used ETL materials (e.g., TiO$_2$, ZnO, SnO$_2$, etc.) and the conduction band minimum (CBM) of general perovskite materials have energy-level-matching issues, which are not conducive to efficient electron extraction and transport, and thus impact the performance of the cells.[59] By altering the interface between the ETL and the perovskite layer, the energy-level structure can be matched to promote the separation and collection of photogenerated charge carriers, preventing the electrons from recombining with the holes.

High-performance PSCs usually require a flat, uniform, dense, and well-crystallized film of the light-absorbing layer as well as the transmission layer. For example, TiO$_2$ is a commonly used ETL material, but there are many oxygen vacancies and defect states on its surface, and the photogenerated electrons will not be able to form photocurrents due to severe recombination with holes, leading to significant performance degradation.[60] It is widely known that when perovskite thin films

are prepared using a fast crystallization technique, defects on the material surface or at the grain boundaries frequently arise, which will enhance non-radiative recombination thus reducing the charge carrier lifetime, causing energy loss and affecting the efficiency of the cells. Furthermore, defects not only promote water–oxygen penetration and accelerate perovskite decomposition but also provide a major pathway for ion migration. Therefore, it is imperative to reduce defects to form a high-quality thin film.[28,31,61] Therefore, interfacial engineering is important to reduce the photo-degradation of perovskite layers caused by external factors (e.g., water, oxygen, and light) and internal factors (e.g., ion migration, electron migration, and interfacial reactions) to obtain efficient and stable PSCs. In the following subsections, we will elaborate on the classification according to the type of material chosen, which are mainly two-dimensional materials, fullerenes and derivatives, quantum dots, self-assembled molecules, inorganic salts and organic materials.

3.2.1 **Two-dimensional (2D) materials.** 2D materials (which mainly include graphene and its derivatives, MXenes, graph-diyne, etc.) are often used to enhance the shape and crystallinity of perovskite materials and enhance charge extraction from the perovskite to the ETL because of their superior optical, electrical, thermodynamic, physical, and catalytic properties.[62–64] It is worth mentioning that a new member of the 2D material family, i.e., MXenes, which have a layered structure formed via selective hydrofluoric acid (HF) or in situ-induced HF corrosion of A (Al, Sn, etc.) layers of the MAX phase (laminated carbides

13616 | J. Mater. Chem. C, 2022, **10**, 13611–13645

This journal is © The Royal Society of Chemistry 2022

and nitrides with a hexagonal closed-packing structure), which possess a higher electrical conductivity than the reduced graphene oxide as well as a lower absorbance in the visible-light range.[65] A typical MXene is $Ti_3C_2T_x$, which has many excellent properties, including a high electronic conductivity, a high mobility and a high charge carrier density. $Ti_3C_2T_x$ with various end groups (T_x) has been used to modify the work function (WF) between the perovskite active layer and the TiO_2 ETL.[66] Ultraviolet photoemission spectroscopy (UPS) observations and density functional theory (DFT) calculations have confirmed that $Ti_3C_2T_x$ optimized the energy band alignment between the TiO_2 ETL and the perovskite layer by inducing the formation of interface dipoles (Fig. 5a–d). Reduction of the WF and the optimization of the energy bands between the TiO_2 ETL and the perovskite layer led to a substantial improvement in the

performance, with a 26% increase in performance compared with control cells without the MXene.

As a new all-carbon nanostructured material after fullerenes, carbon nanotubes, and graphene, graphdiyne (GDY) is gradually being applied in the field of optoelectronic semiconductors because of its favorable charge transport capabilities and excellent semiconductor properties.[67] Zhang *et al.* utilized GDY to effectively increase the power-level matching between the SnO_2 ETL and the perovskite layer, resulting in a 4-fold increase in electron mobility.[68] High-quality perovskite films with low defect density were also formed through interfacial modification using GDY. Systematic DFT studies further explained that the underlying mechanism is the facilitation of charge extraction and transport through the coupling of GDY and SnO_2. By modifying the SnO_2/perovskite interfaces with GDY, the final device
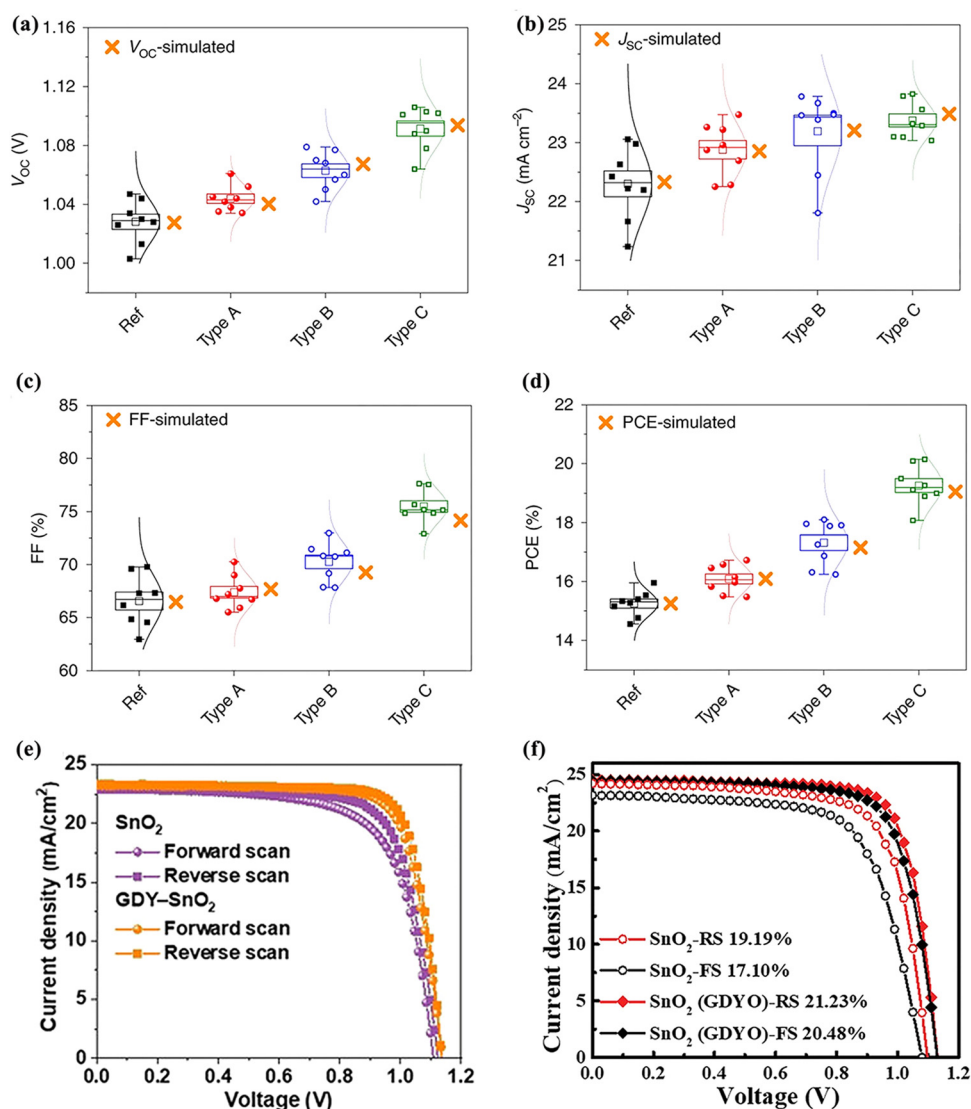

Fig. 5 Two-dimensional materials for the ETL/perovskite interface of normal structural PSCs. (a)–(d) Statistics of the photovoltaic parameters based on pristine and different post-processing of MXene. Reproduced with permission from ref. 66. Copyright 2019 Springer Nature. (e) *J*–*V* curves of PSCs based on SnO_2 and SnO_2/GDY. Reproduced with permission from ref. 68. Copyright 2020 Wiley. (f) *J*–*V* curves of PSCs based on SnO_2 and SnO_2/GDYO. Reproduced with permission from ref. 69. Copyright 2021 The Royal Society of Chemistry.

This journal is © The Royal Society of Chemistry 2022

J. Mater. Chem. C, 2022, **10**, 13611–13645 | **13617**

obtained a 21.11% efficiency with negligible hysteresis (Fig. 5e). Similarly, graphdiyne oxide (GDYO) was also applied to modify the SnO_2 ETL.[69] GDYO can passivate the surface defects of SnO_2 to enhance electron transport while inhibiting non-radiative recombination due to the content of hydrophilic carboxyl and hydroxyl functional groups that can establish chemical interactions with uncoordinated Sn. The WF of GDYO-modified SnO_2 matched well with perovskite, leading to a higher PCE of 21.23% in the final device (Fig. 5f). After 24 days of holding at 80 °C, the unencapsulated device efficiency declined to 84%, and after 160 hours of continuous light illumination, it reduced to 71%.

3.2.2 Fullerene (C_{60}) and derivatives. Fullerene (C_{60}) and its derivatives have great potential as interfacial modification layers because of their high electron mobility, tunable energy levels, and low-temperature film formation. The interface problem between the metal oxide and perovskite layers is one of the major issues for the performance limitation of PSCs, so the rational design of C_{60} molecules with excellent electrical properties and adaptable chemical parts for interfacial modification is greatly required. The theoretical mechanism of C_{60} as an interfacial modification layer has been explored.[70] The lowest unoccupied molecular orbital (LUMO) energy level of C_{60} is less than the conduction band (CB) of TiO_2, which enables a better energy-level matching of the device. In addition, C_{60} also passivates the surface trap states, and has a positive impact on the carrier lifespan, charge injection, and separation (Fig. 6a and b). Specifically, C_{60} was discovered to be capable of extracting the hot carriers formed during the initial timescale of photoexcitation, making it appropriate for hot-carrier PSCs.

Novel fulleropyrrolidine (NMBF-X, where X = H or Cl) monomers and dimers were inserted between the metal oxide ETL and the perovskite layer to form an interfacial modification
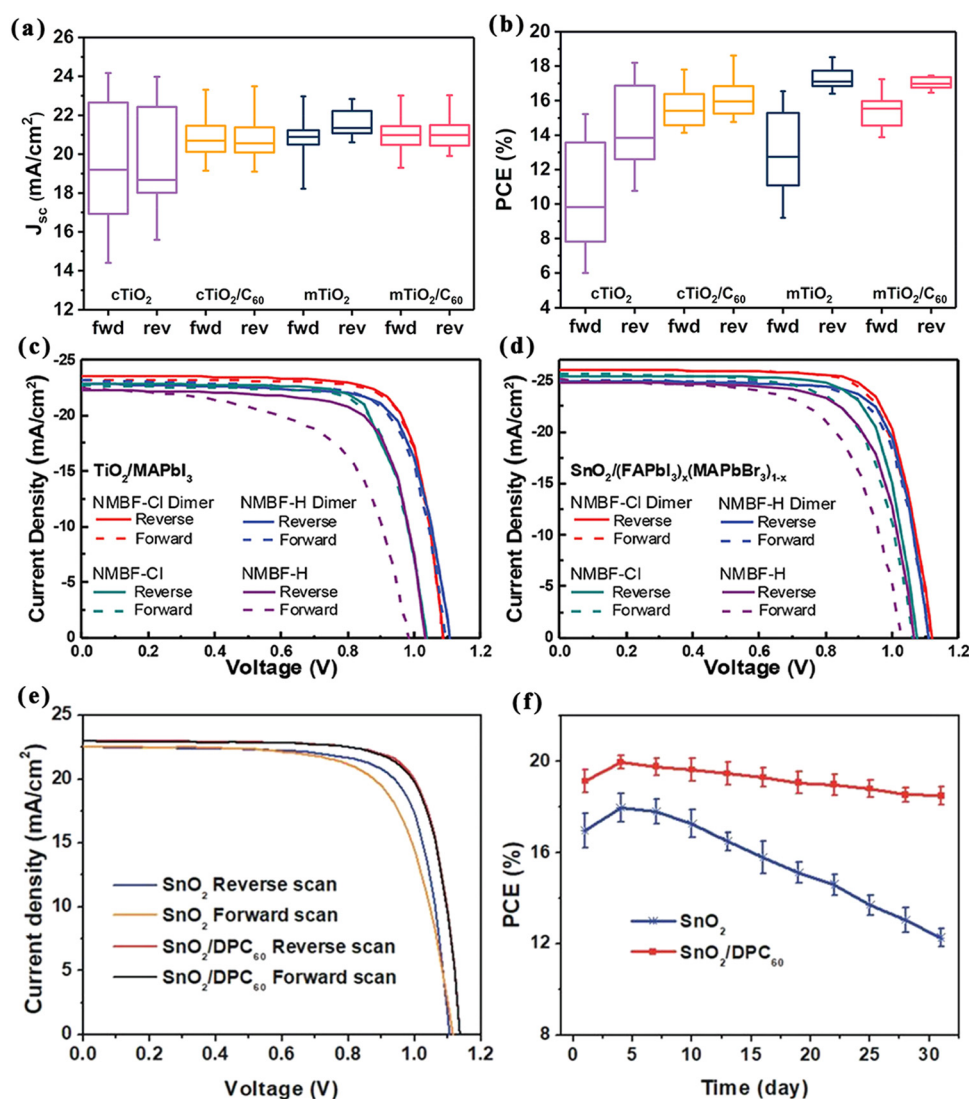

Fig. 6 Fullerene (C_{60}) and derivatives for ETL/perovskite interfaces of normal structured PSCs. (a) and (b) Photovoltaic parameters of C_{60}-based PSCs. Reproduced with permission from ref. 70. Copyright 2020 American Chemical Society. (c) and (d) *J−V* curves of PSCs based on TiO_2 and SnO_2/NMBF−X monomers and dimers. Reproduced with permission from ref. 71. Copyright 2020 Wiley. (e) and (f) *J−V* curves of PSCs based on SnO_2 and SnO_2/DPC_{60} and measured curves of environmental stability. Reproduced with permission from ref. 72. Copyright 2019 Wiley.

13618 | *J. Mater. Chem. C*, 2022, **10**, 13611–13645

This journal is © The Royal Society of Chemistry 2022

layer.[71] The ETLs were TiO$_2$ and SnO$_2$, and the perovskite materials were chosen as MAPbI$_3$ and (FAPbI$_3$)$_x$(MAPbBr$_3$)$_{1-x}$. After modifying the ETL/perovskite interfaces with fulleropyrrolidine, the device performance increased significantly (Fig. 6c and d). The chlorinated fullerene dimer was found to coordinate more effectively with metal oxides and perovskites through chloride terminations, resulting in excellent stability and an efficiency enhancement. This unencapsulated planar device achieved an efficiency of 22.3% without hysteresis. More importantly, the initial efficiency of over 98% was maintained after 1000 hours of environmental storage.

Similarly, a fullerene derivative with amine functional groups, i.e., 2,5-diphenyl C$_{60}$ fulleropyrrolidine (DPC$_{60}$), was introduced as an interfacial layer between perovskite and SnO$_2$.[72] Owing to its unique structure and functional groups, DPC$_{60}$ can interact with the perovskite, passivating the interfacial defects of the perovskite layer. Meanwhile, better energy-level matching led to a substantial increase in electron extraction. Therefore, a PSC with the addition of DPC$_{60}$ achieved a PCE of 20.4%, which is higher than the control device (18.8%) (Fig. 6e and f). In addition, the hydrophobic DPC$_{60}$ layer significantly increased the stability, maintaining an initial efficiency of 82% after continuous exposure under one sun illumination and thermal aging (55 $\pm$ 5 $^\circ$C) for 200 h.

3.2.3 Quantum dots (QDs). With the advantages of bandgap tunability, quantum coherence and edge effects, QDs can be utilized as interfacial modification materials. For example, inorganic colloidal QDs are a class of uniformly distributed inorganic nanoparticles with functional groups or ionic passivation on the surfaces. The ultra-small particle size (a few nanometers) enables QDs to be well dispersed on the surfaces of the CTL to repair pores, while the functional groups on the surfaces of the QDs have the potential to passivate defects at the CTL/perovskite interfaces. One typical example is SnO$_2$-QDs synthesized using precursor solutions containing SnCl$_2$ and thiourea.[73] SnO$_2$-QDs capped with chloride ions were added to the spin-coated TiO$_2$ ETL/perovskite interface to fill the vacancies on the ETL and passivate the defects with chloride ions at the TiO$_2$/perovskite interface. In addition, both photoluminescence spectroscopy and electrochemical impedance spectroscopy demonstrated that the SnO$_2$-QDs can effectively improve charge extraction and suppress interfacial charge recombination. Consequently, the PSCs derived using SnO$_2$-QDs achieved a champion performance of 17.3% and outstanding long-term stability under continuous light exposure (Fig. 7a and b). Apart from SnO$_2$-QDs, Hui et al. described a composite ETL that consisted of carboxylic-acid- and hydroxyl-rich red-carbon quantum dots (RCQs) doped with low-temperature solid solution-treated SnO$_2$ that showed an approximately 20-fold increase in electron mobility, ranging between 9.32×10^{-4} and 1.73×10^{-2} cm^2 V^{-1} s^{-1}.[74] The PSCs based on this new ETL exhibited a PCE of up to 22.77% and excellent stability, maintaining an initial efficiency of 95% at 25 $^\circ$C and 40–60% air humidity (Fig. 7c and d).

A recent study showed that MXene quantum dot-modified SnO$_2$ can modulate the crystallization process of the perovskite for preparing effective and reliable PSCs, and the crystallization kinetics were explored for the first time using a synchrotron-based 2D grazing incidence X-ray diffraction technique.[75] It was found that titanium carbide (Ti$_3$C$_2$)-MXene quantum dot-modified SnO$_2$ (MQDs-SnO$_2$) could rapidly induce perovskite nucleation in the precursor solutions and form intermediate perovskite phases after antisolvent treatment, thus improving the crystalline quality and phase stability of the perovskite films. The optimal performance of the corresponding PSCs reached 23.3% with excellent moisture resistance and photostability (Fig. 7e and f).

Shortly thereafter, Gao et al. proved the role of imidazole bromide functionalized graphene quantum dots (I-GQDs) in regulating the ETL and the perovskite layer (FAPbI$_3$).[76] Better energy-band docking can be achieved via modification of the I-GQDs for reducing charge accumulation and promoting electron transport. Furthermore, the surface functional groups of the I-GQDs facilitated the formation of high-quality perovskite films to decrease the non-radiative recombination within the films. Furthermore, the material can enhance the stability of PSCs without modifying the band gap of the FA-based perovskite layer due to strong interactions between the imidazole moiety at the surface of I-GQDs and the perovskite. As a result, an improved PCE of 22.37% was achieved, and better long-term stability was obtained (Fig. 7g and h).

3.2.4 Self-assembled molecules (SAMs). Self-assembled single molecules (SAMs) have emerged as excellent nanomaterials for improving the performance of PSCs due to the ability to control their chemical and physical interfacial properties. In fact, numerous reports in recent years have confirmed that using SAMs for PSCs can significantly improve the device performance.[77–79] Han et al. designed methoxybenzoic acid self-assembled monolayers (SAMs) to passivate the ZnO ETL surface, thereby improving the photovoltaic performance and stability of the device.[80] The device structure is ITO/ZnO/(SAMs)/CH$_3$NH$_3$PbI$_3$/spiro-OMeTAD/Au, where the SAMs are 4-methoxybenzoic acid (MBA), 3,4-dimethoxybenzoic acid (DMBA), and 3,4,5-trimethoxybenzoic acid (TMBA), respectively (Fig. 8a). It was found that TMBA has a stronger dipole moment and bonding between methoxy hydrogen and ammonium compared with MBA and DMBA, which effectively enhanced the electron transport between the perovskite layer and the ETL. In addition, the methoxy in TMBA increased the surface hydrophobicity of the ZnO ETL, and the optimal device efficiency was raised by 13.75% when it was designed using ZnO/TMBA. More importantly, the incorporated interfacial modification layer significantly improved the stability of the PSCs under environmental circumstances by blocking the proton transfer process between the ETL and the perovskite layer (Fig. 8b and c). Likewise, a SAM of 3-mercaptopropyltrimethoxysilane (MPTMS) was reported as a new interfacial layer to increase the quality of the light-absorbing layer and promote the extraction of photogenerated electrons (Fig. 8d).[81] The average PCE of such PSCs utilizing MPTMS was significantly increased from 16.62% to 18.75% in the device prepared via a two-step process. The modified PSC obtained a maximum efficiency of more than 20% with favorable stability in ambient air (Fig. 8e and f).

This journal is © The Royal Society of Chemistry 2022

J. Mater. Chem. C, 2022, **10**, 13611–13645 | **13619**

Fig. 7   QDs for the ETL/perovskite interfaces of normal structural PSCs. J–V curves (a) and stability curves (b) of PSCs based on pristine and SnO_2-QDs. Reproduced with permission from ref. 73. Copyright 2019 Elsevier. J–V curves (c) and stability curves (d) of PSCs based on SnO_2 and SnO_2-RCQs. Reproduced with permission from ref. 74. Copyright 2020 Wiley. J–V curves (e) and stability curves (f) of PSCs based on SnO_2 and SnO_2/MQDs. Reproduced with permission from ref. 75. Copyright 2021 The Royal Society of Chemistry. J–V curves (g) and stability curves (h) of PSCs based on SnO_2 and SnO_2/I-GQDs. Reproduced with permission from ref. 76. Copyright 2021 Wiley.

An iodine-terminated self-assembled molecule (I-SAM, *i.e.*, $[Si(OCH_3)_3(CH_2)_3I]$) was adopted as the interfacial modifier, while $[Si(OCH_3)_3(CH_2)_3H]$ was applied as the control molecule to investigate the role of iodine as an end-group atom (Fig. 8g).[82] The silane structure in this molecule can be modified well at the interface as a SAM layer structure, while eliminating the –OH groups at the interface by reacting with them. This resulted in a 50% increase in the mechanical bond strength of the ETL/perovskite compared with $[Si(OCH_3)_3(CH_2)_3H]$. The efficiency of the device modified using the I-SAM increased from 20.2% to 21.4%. In addition, the results for the long-term operating stability of the PSCs at the maximum efficiency point proved that its T_{80} (lifetime to maintain 80% of the initial efficiency) was projected to increase from 700 h to 4000 h (Fig. 8h and i).

3.2.5   Inorganic salts. Alkali halides have been effectively employed in the manufacture of interfacial layers.[83] For instance, Azmi *et al.* passivated organic–inorganic hybrid perovskite (OIHP) crystals and defects at the ETL/OIHP interface by incorporating Cl^- (LiCl, NaCl, KCl, and CsCl).[84] Low-temperature treated PSCs (L-PSCs) with excellent long-term

stability and high efficiency were designed. The experimental results pointed out that the best performance of L-PSC-KCl exhibited an efficiency of 22.6%. More importantly, a large-area device with outstanding properties (21.3%, 1.12 cm^2) was obtained using the excellent homogeneous modification technique.

Vacancy defects can lead to the occurrence of ion migration. By inducing a local chemical doping effect, the Fermi energy level in the ion aggregation zone moves away from the conduction/valence band as a result of ion migration, causing a bending of the energy level, which affects the separation, transport and extraction of carriers, ultimately degrading the performance of the device. I^- has been proved to have the shortest migration path in the $MAPbI_3$ perovskite, while Pb^{2+} is difficult to migrate.[85,86] $NdCl_3$ as an interfacial modification layer was systematically studied.[87] It demonstrated that the $NdCl_3$ interfacial layer ($NdCl_3$-IL) fills the I^- vacancies resulting in a reduction of the vacancy and an increase in the activation energy, which inhibits the migration of I^- from the top surface to the rear interface, thus reducing the trap density (Fig. 9a). The device modified using this interfacial layer obtained a PCE

Fig. 8 SAMs for ETL/perovskite interfaces of normal structural PSCs. Schematic diagram of the structure of (a) MBA (left), DMBA (middle), and TMBA (right), (d) MPTMS, and (g) I-SAM. *J*–*V* curves ((b), (e) and (h)) and stability curves ((c), (f) and (i)) of PSCs based on ZnO, ZnO/MBA, ZnO/DMBA and ZnO/TMBA (b) and (c), pristine ETL SnO_2 and SnO_2/MPTMS (e) and (f), and pristine ETL SnO_2 and with ETL H-SAM or I-SAM (h) and (i). (a)−(c) Reproduced with permission from ref. 80. Copyright 2020 The Royal Society of Chemistry. (d)−(f) Reproduced with permission from ref. 81. Copyright 2021 Wiley. (g)−(i) Reproduced with permission from ref. 82. Copyright 2021 The American Association for the Advancement of Science.

of 22.16% and a higher V_{oc} with a negligible hysteresis effect. The stability of the device was also improved, maintaining 83% of the initial performance after 100 hours of the maximum power point tracking test. Notably, the method in combination with the 2D/3D passivation strategy was applied to a large-area (1cm^2) device, obtaining a certified efficiency of 21.68%.

Monovalent Cu cations (Cu$^+$) were also utilized to solve the problems of low electron mobility, poor electrical conductivity, and the possibility of acting as a photocatalyst for chemical reactions in TiO$_2$.[88] The uniform distribution of Cu$^+$ not only increased the extraction rate of photogenerated carriers but also reduced the surface trap states, thus improving the device

performance. The final obtained planar PSCs achieved a PCE of 18.15%, which was better than 15.78% for the blank device (Fig. 9b). To verify the generalizability, the method was applied to mesoporous structures, and the experimental results proved the same modification capability. Notably, aging tests as well as stability experiments demonstrated that the Cu-modified device exhibited superior long-term stability.

Another effective strategy was to utilize CsI-doped SnO$_2$, thus effectively improving the SnO$_2$/perovskite interfacial quality of the PSCs.[89] The presence of CsI during the formation of perovskite films passivated the interfacial imperfections. In addition, the gradient distribution of Cs$^+$ contributed to a more
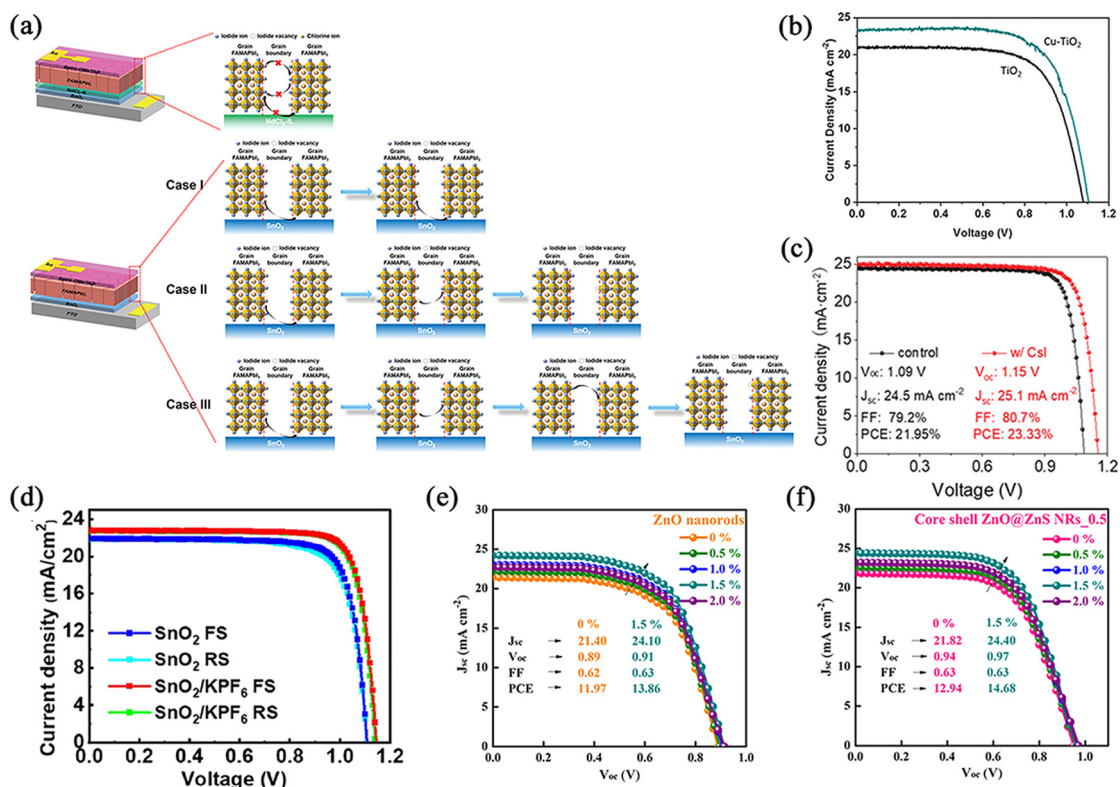
This journal is © The Royal Society of Chemistry 2022

J. Mater. Chem. C, 2022, **10**, 13611–13645 | **13621**

Fig. 9 Inorganic salts for ETL/perovskite interfaces of normal structural PSCs. (a) Diagram of I⁻ migration in control and NdCl₃-IL-based PSCs. Reproduced with permission from ref. 87. Copyright 2021 Wiley. (b) J–V curves of PSCs based on TiO₂ and Cu–TiO₂. Reproduced with permission from ref. 88. Copyright 2021 Elsevier. (c) J–V curves of PSCs based on SnO₂ and SnO₂/CsI. Reproduced with permission from ref. 89. Copyright 2021 Wiley. (d) J–V curves of PSCs based on SnO₂ and SnO₂-KPF₆. Reproduced with permission from ref. 90. Copyright 2021 Elsevier. (e) and (f) J–V curves of PSCs based on ZnO (e) and ZnO–ZnS (f) on flexible substrates. Reproduced with permission from ref. 92. Copyright 2021 Elsevier.

acceptable energy-band alignment of SnO₂ with the perovskite. The resistance of FAPbI₃-based PSCs to UV irradiation was enhanced after doping with Cs⁺, achieving an excellent efficiency of up to 23.3% (Fig. 9c).

The importance of KPF₆ for modification of the SnO₂/perovskite interface was also demonstrated.[90] It was found that PF₆⁻ remained at the interface while most of the K⁺ ions diffused into the perovskite. In addition, PF₆⁻ formed hydrogen bonds with organic cations in the perovskite component, and coordination bonds with SnO₂, which can effectively passivate interfacial defects and release interfacial stresses. The PCE of the device obtained using KPF₆ was increased from 19.66% to 21.39%, and the unencapsulated device maintained its initial efficiency of 80.1% after 960 hours of aging at 60 °C (Fig. 9d). Similarly, multifunctional potassium sulfate (K₂SO₄) was also used as an interface modification material for SnO₂/perovskite.[91] K₂SO₄ achieved the goals of both defect passivation and optimized energy-band alignment owing to the synergistic interfacial and internal modification of the perovskite. With the modification of K₂SO₄, the photovoltaic performance was increased from 19.45% to 21.18%. Moreover, the initial efficiency values of the modified PSCs can be maintained above 85% after storage at 25% relative humidity for 1000 hours.

More recently, interfacial engineering has been continuously devoted to the study of wearable and portable flexible PSCs.

Fahim *et al.* explored the modification process after the ZnO surface was converted to ZnS.[92] The bifunctional interfacial layer reduces the hydroxyl (–OH) groups on the ZnO surface, and passivates the ZnO/perovskite interface, thereby improving the stability. It also modulated the energy level for effective electron transport through the strain-induced piezoelectric effect (Zn–S–Pb pathway). The piezoelectric effect regulates the energy band structure through the internal piezoelectric potential generated by the piezoelectric semiconductor under pressure, controlling the separation, transport and recombination of excitons.[93,94] As a result, the efficiency of the flexible PSC was dramatically improved (Fig. 9e and f).

3.2.6 Organic materials. Organic materials such as organic small molecules, organic ammonium salts, and polymers are widely recognized as an important source of interfacial modification materials. Different concentrations of 2-methylbenzimidazole (MBIm) were introduced between the SnO₂ ETL and the perovskite photoactive layer to address the problem of non-radiative recombination loss due to interfacial defects.[95] The researchers emphasized the importance of this passivation mechanism, and the MBIm molecule not only optimized the energy-level-matching problem and reduced the photovoltage loss but also passivated the interfacial defects by forming Lewis adducts that bind to uncoordinated Pb²⁺, minimizing non-radiative recombination. Ultimately, the efficiency was significantly increased from 19.5%

13622 | *J. Mater. Chem. C*, 2022, **10**, 13611–13645

This journal is © The Royal Society of Chemistry 2022

to 21.6% with a significant rise in V_{oc} ($\sim$90 mV). In particular, the device preserved 85% and 90% of the initial efficiency under high-humidity and continuous-light conditions, respectively.

In another study, Sun *et al.* employed the amphiphilic linker molecule *p*-aminobenzenesulfonic acid (ABSA) at the interface of the SnO$_2$/perovskite.[96] The authors explained the mechanism of the interfacial modification in terms of energy-band bending. Both experimental and theoretical studies comprehensively demonstrated that the sulfonic acid group of ABSA can modify the SnO$_2$, thus reducing the energy-band potential barrier on the surface of the ETL and enhancing the charge transport. The alkaline amino groups were used to passivate deep-energy-level defects on the perovskite surface and reduced non-radiative recombination. The PCE of MAPbI$_3$-based PSCs modified with this material was significantly improved from 18.02% to 20.32% with better long-term stability.

Although fullerenes and their derivatives dominate the organic photovoltaic field due to their unique structure and other advantages, the material itself has some insurmountable drawbacks, however, such as a low absorption in the visible range, difficulties with modification, and high cost, all of which restrict the device performance and wide-scale use. In recent years, the emergence of non-fullerene-type small-molecule materials, especially the Y series of non-fullerenes (Y-NFAs; mainly Y1–Y6), has attracted increasing attention from the scientific community.[97] For example, Lou *et al.* designed the

Y-series derivative BTAC$_4$ to modify the SnO$_2$ layer *via* side-chain engineering.[98] An efficiency of more than 23% was achieved. By exploring the interaction between the π-conjugated n-type small molecules and the SnO$_2$/perovskite interfaces, the team revealed the outstanding interfacial modification effect of organic passivators with a more compact and ordered molecular filling ability.

In the same year, Kong *et al.* demonstrated that doping EDTA-2M molecules (M = K, Rb, or Cs) with SnO$_2$ colloids improved the electrical and surface properties of the SnO$_2$ films, resulting in a substantial increase in electron mobility.[99] In addition, EDTA-2M molecules can successfully passivate the surface imperfections of SnO$_2$ and improve its crystalline quality by promoting perovskite crystallization. The PCE of the device with perovskite band gaps of 1.69 eV and 1.57 eV, respectively, reached up to 23.30%. Unencapsulated PSCs on the basis of EDTA-modified SnO$_2$ were maintained at 95% of their initial performance after exposure to an ambient atmosphere for 1200 h.

Shortly thereafter, (2-carboxyethyl)(dimethyl)sulfonium chloride (CDSC) and 3-(dimethylamino)propionic acid hydrochloride (DPAH) (reference molecule) were employed to modify the SnO$_2$/perovskite interfaces.[100] It was theoretically and experimentally proved that the CDSC and DPAH molecules are capable of strong chemical interactions with both SnO$_2$ and the perovskite layer, thus linking the two through chemical bonding and improving interfacial contacts. Both salt molecules were able to
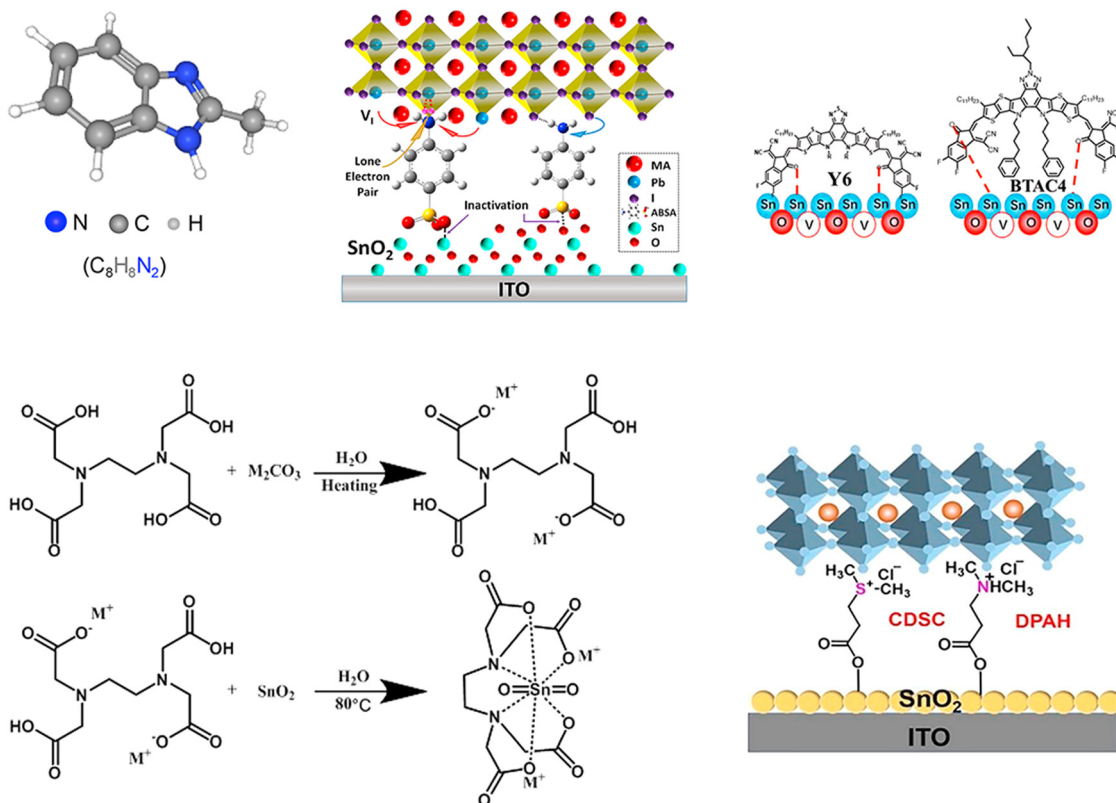

Fig. 10 Structure diagram of various organic molecules for the ETL/perovskite interface of normal structural PSCs. Reproduced with permission from ref. 95–98 and 100. Copyrights 2020, 2021, 2022 Elsevier, 2021 American Chemical Society, and 2021 Wiley.

This journal is © The Royal Society of Chemistry 2022

J. Mater. Chem. C, 2022, **10**, 13611–13645 | **13623**

effectively passivate defects from the surface of the perovskite and the ETL, and the CDSC-modified device achieved a higher PCE (22.22%) as well as better stability. The structures of the small organic molecules used for normal structural PSCs are shown in Fig. 10.

To address the severe charge-trap problem in perovskite films, 1-butyl-3-methylimidazolium tetrafluoroborate ([BMIM]BF$_4$) and triphenylphosphine oxide (TPPO) were synergistically applied to PSCs.[101] [BMIM]BF$_4$ formed an interfacial dipole layer that reduced the surface WF of the ETL and filled the organic/Cs cation vacancies. The P=O bond in the TPPO molecule interacts with the uncoordinated Pb^{2+}, which reduced the defect states in the perovskite films and reduced the non-radiative recombination. As a result, the PCE of the PSC increased from 18.7% to 21.1% with long-term stability, even under dry air conditions (about 22% relative humidity at 25 °C).

ZnO possesses excellent optoelectronic properties, it can be prepared at low temperatures, and it has a higher electron mobility than TiO$_2$, thus attracting much attention.[102,103] However, since ZnO is an amphoteric oxide with an extremely unstable surface, it tends to react with MAI for the preparation of perovskites, leading to an increment in interfacial defects in the perovskite layer, which increases the carrier recombination and induces degradation of the optoelectronic performance of the device.[104] Methylammonium iodide can be used to solve this problem by modifying the ETL.[105] It was shown that methylammonium iodide modification can effectively block the reaction between ZnO and the perovskite layers. The obtained PSCs exhibited excellent thermal stability, and retained 82% of the initial efficiency after aging at 50 mW cm^{-2} of white light and 65 °C for 2100 hours, which is the highest known performance.

Adhesion of the weakly alkaline precursor of biguanide hydrochloride (BGCl) on the surface of the tin oxide substrate can significantly improve the denseness and uniformity of the tin oxide layer.[106] At the same time, the amino group in BGCl can undergo Lewis coordination with Sn^{4+} to achieve n-type doping of tin oxide, while the Cl$^-$ effectively passivates the oxygen vacancy defects in the surface layer through electrostatic coupling. In addition, the amino and ammonium functional groups enriched with BGCl can effectively anchor I$^-$ in the solution of the perovskite precursor, ensuring the growth of the perovskite with an ordered array arrangement and a vertical crystallographic orientation. Therefore, carrier extraction at the interface was significantly enhanced, achieving better carrier transport inside the device. The prepared devices achieved up to 24.4% certified PCE and long-term stability.

It is worth noting that organic interfacial layers can also be applied to flexible PSCs. You *et al.* designed a biological polymer (heparin potassium, HP) as an SnO$_2$–HP composite layer to enhance the interfacial contact between the ETL and the perovskite layer.[107] On the one hand, owing to the interaction between the Sn atoms of SnO$_2$ and the O atoms of –COO–, HP is able to adhere to the surface of the SnO$_2$ nanocrystals. On the other hand, the polymerization chain of HP could attenuate the interaction between the adjacent SnO$_2$ nanocrystals and promote their uniform dispersion. Meanwhile, because of the

larger domains and higher surface free energy of the SnO$_2$–HP layer, the perovskite may undergo more uniform crystal nucleation, which leads to better growth of the perovskite crystals. The SnO$_2$–HP-based device exhibited a highly reproducible average efficiency of 23.03% and excellent operating stability on the rigid substrate. More importantly, the average efficiency of the HP-modified SnO$_2$ ETL on flexible substrates is 19.47%, showing excellent potential for flexible and large-area device studies.

Xiong *et al.* reported poly(ethylene glycol) diacrylate (PEGDA) as a polymer backbone for modifying SnO$_2$.[108] The ETL treated with this material showed a significant impact on both the device performance and stability. On the one hand, more homogeneous and energy-level-aligned interfaces were achieved, increasing the electrical conductivity. On the other hand, PEGDA can passivate the defects at the ETL/perovskite interfaces. The final device achieved a champion photovoltaic performance of 23.31% with excellent stability. Typical modification materials that can enhance both the device performance and stability in this interface are screened and summarized in Table 1.

3.3 Perovskite/HTL interface

Similar to the ETL, it is vital to establish effective hole injection and stable transport in order to generate high-efficiency PSCs. Too large a gap between the HTL and the energy band of the perovskite layer can lead to inefficient hole injection into the HTL and a decrease in V_{oc}.[109,110] In addition, there are a large number of defect sites in the perovskite/HTL interface, and these defect sites can capture carriers and cause carrier loss due to recombination.[111] Moreover, these defect sites will become adsorption sites for water oxygen, which will accelerate the decomposition and degradation of the perovskite film and cause rapid degradation of the performance of the PSCs.[112] Optimization at the perovskite/HTL interface is essential to passivate the defects and obtain high-quality films.[59,113] Since the existing hole materials do not fully satisfy the objectives of energy-level alignment, enhanced charge dynamics, trap passivation, and reduced ion migration, interfacial modification has been developed as an effective method for the perovskite/HTL interface.

3.3.1 Two-dimensional materials. Two-dimensional (2D) perovskite materials have a layered structure with alternating organic amine layers and inorganic layers. Compared with conventional three-dimensional (3D) perovskite materials, they are more stable to the environment and have a flexible and adjustable structure. Modifying 2D perovskite layers on the 3D perovskite surface to passivate defects can improve the efficiency of PSCs while ensuring their stability, and the underlying mechanism has also been interpreted.[114] The key to superior optoelectronic characteristics and carrier dynamics of PSCs at the 2D/3D interface lies in the crystal alignment of the 2D perovskite. If the arrangement is 'flat' with regard to the substrate, it can potently passivate interfacial defects while hindering charge recombination. It is worth mentioning that this arrangement can be adjusted *via* fine-tuning the chemical composition of the 2D cations.

13624 | *J. Mater. Chem. C*, 2022, **10**, 13611–13645

This journal is © The Royal Society of Chemistry 2022

Table 1 Modification materials at the ETL/perovskite interface with the ability to simultaneously improve the efficiency and stability of normal structured PSCs

Modification materials		Perovskite	Main roles	PCE [%]	Stability	Ref.
Two-dimensional materials	GDYO	$(FAPbI_3)_{1-x}(MAPbBr_3)_x$	Facilitate electron transport, suppresses non-radiative recombination	21.23	84% of initial efficiency after 24 d at 80 °C	69
Fullerene (C_{60}) and derivatives	NMBF-X	$(FAPbI_3)_x(MAPbBr_3)_{1-x}$	Better coordination with ETL and perovskite	22.3	Over 98% of initial efficiency after 1000 h of storage	71
	DPC$_{60}$	$FA_{0.81}MA_{0.10}Cs_{0.04}PbI_{2.55}Br_{0.40}$	Passivate interface defects, improve electron extraction	20.4	82% of initial efficiency after 200 h of continuous sunlight exposure and thermal aging (55 ± 5 °C)	72
Quantum dots (QDs)	RCQs	$Cs_{0.05}(MA_{0.17}FA_{0.83})_{0.95}Pb(I_{0.83}Br_{0.17})_3$	Improve electromigration	22.77	95% of initial efficiency at 25 °C and 40–60% air humidity	74
	MQDs	$FA_{0.9}MA_{0.05}Cs_{0.05}PbI_{0.98}Br_{0.02}$	Improve crystalline quality and phase stability of perovskite films	23.3	Over 90% of initial efficiency after 500 h of continuous light exposure	75
	I-GQDs	$FAPbI_3$	Improve energy-level matching and quality of perovskite films	22.37%	84% of initial efficiency after 600 h	76
Self-assembled molecules (SAMs)	I-SAM	$Cs_{0.05}(FA_{0.85}MA_{0.15})_{0.95}Pb(I_{0.85}Br_{0.15})_3$	Increase the mechanical bonding strength of the interface	21.4	Projected T_{80} from 700 h to 4000 h	82
Inorganic salts	NdCl$_3$	$FA_{1-x}MA_xPbI_3$	Inhibit the migration of I$^-$	22.16	83% of initial efficiency after 100 h of maximum power point tracking testing	87
	Cu^{1+}	$MAPbI_3$	Improve extraction of carriers, reduce surface trap states	18.15	53% of the initial efficiency under aging test conditions, 91% of initial efficiency under light stabilization experimental conditions	88
	KPF$_6$	$Rb_{0.05}(FA_{0.95}MA_{0.05})_{0.95}PbI_{2.85}Br_{0.15}$	Improvement of perovskite film quality, passivate interface defects, release interfacial stresses	21.39	80.1% of initial efficiency after 960 h of aging at 60 °C and 57.2% after 960 h of exposure to 1 Sun illumination	90
Organic materials	MBIm	$Cs_{0.05}(MA_{0.15}FA_{0.85})_{0.95}Pb(I_{0.85}Br_{0.15})_3$	Optimize energy-level matching, passivate interface defects, reduce non-radiative recombination	21.6	85% and 90% of initial efficiency under high-humidity and continuous-light conditions	95
	ABSA	$MAPbI_3$	Enhance charge transport, passivate defects, reduce non-radiative recombination	20.32	56.7% of the initial efficiency after 30 d in the atmosphere	96
	EDTA-2M	$FA_{0.95}MA_{0.05}Pb(I_{0.95}Br_{0.05})_3$	Passivate interface defects and improve the crystalline quality of perovskite	23.30	95% of initial efficiency after 1200 h in the atmosphere	99
	CDSC	$Rb_{0.02}(FA_{0.95}Cs_{0.05})_{0.98}PbI_{2.91}Br_{0.03}Cl_{0.06}$	Passivate interface defects	22.22	92.5% of initial efficiency after aging at 60 °C for 1272 h	100
	[BMIM]BF$_4$ and TPPO	$Cs_{0.05}(MA_{0.17}FA_{0.83})_{0.95}Pb(I_{0.83}Br_{0.17})_3$	Reduce surface WF of ETL and non-radiative recombination	21.1	98.3% of initial efficiency after 214 d under dry air conditions	101
	BGCl	$(FAPbI_3)_x(MAPbI_3)_y$	Enhance extraction and transport of carriers	24.4	95% of initial efficiency with over 500 h of aging	106
	HP	$Cs_{0.05}FA_{0.85}MA_{0.10}Pb(I_{0.97}Br0_{.03})_3$	Improve the growth of perovskite crystals, promote the uniform dispersion of SnO$_2$	23.03	97% of the initial efficiency after 1000 h under 1 Sun illumination	107
	PEGDA	$FAPbI_3$	Increase electrical conductivity, passivate interface defects	23.31	Over 90% of initial efficiency with 850 h of continuous lighting	108

It has recently been reported that the modification effect of the 2D structure is affected by the length of its alkyl chain.[115] Furthermore, the surface defects of the 2D perovskite films themselves may also be related to the interaction of their structures with the HTL. In this study, a 3D perovskite was treated with 2D structures of butylammonium iodide (BAI), octylammonium iodide (OAI) and dodecylammonium iodide (DAI) with different alkyl chain lengths, and the PCE and humidity stability of the devices were compared. The results revealed a significant improvement in the electron-blocking ability and humidity resistance as the alkyl chain length was increased from BA to OA to DA. The OAI-treated PSC obtained a champion PCE of 22.9% in comparison with the other two materials.

Similarly, Liu *et al.* focused on an interfacial passivation strategy of a 2D perovskite.[116] Four structured aromatic organic cations without halogen functional groups were designed to form low-dimensional perovskite (LDP) passivation layers, namely benzylammonium (BA), 4-fluorobenzylammonium (FBA), 4-chlorobenzylammonium (CBA) and 4-bromobenzylammonium

This journal is © The Royal Society of Chemistry 2022

J. Mater. Chem. C, 2022, **10**, 13611–13645 | **13625**

(BBA), with their respective modification effects being investigated (Fig. 11a and b). The various halogenated LDP passivation layers exhibited different effects due to their unique crystal parameters and chemical properties. The experimental results demonstrate that all four materials can reduce the non-radiative recombination loss and trap states. Remarkably, the device exhibits significantly enhanced long-term stability under different aging conditions due to the good hydrophobicity of the halogenated LDP and its ability to inhibit organic molecules and iodide ions from diffusing.

The 2D PEA_2PbI_4 layer was found to be used as a passivation layer on 3D perovskite films by Chen et al.[117] This further tuned the Fermi energy level, significantly reduced the trap density on the 3D perovskite surface, and suppressed non-radiative recombination. Final PSCs with an efficiency of 18.51% were obtained. More importantly, the device could maintain an initial efficiency of nearly 90% after 1000 h under high humidity ambient conditions of 60 ± 10%.

In contrast to the above research directions, Long et al. worked out the effect of a 2D perovskite on flexible PSCs.[118] They introduced a 2D perovskite formed from 4-trifluoromethyl-phenylethylamine iodide (CF_3PEAI) on the surface of a 3D perovskite. The 2D perovskite not only improved the energy-level alignment between the HTL and the perovskite layer but also reduced the trap density in the 3D perovskite, lowering the
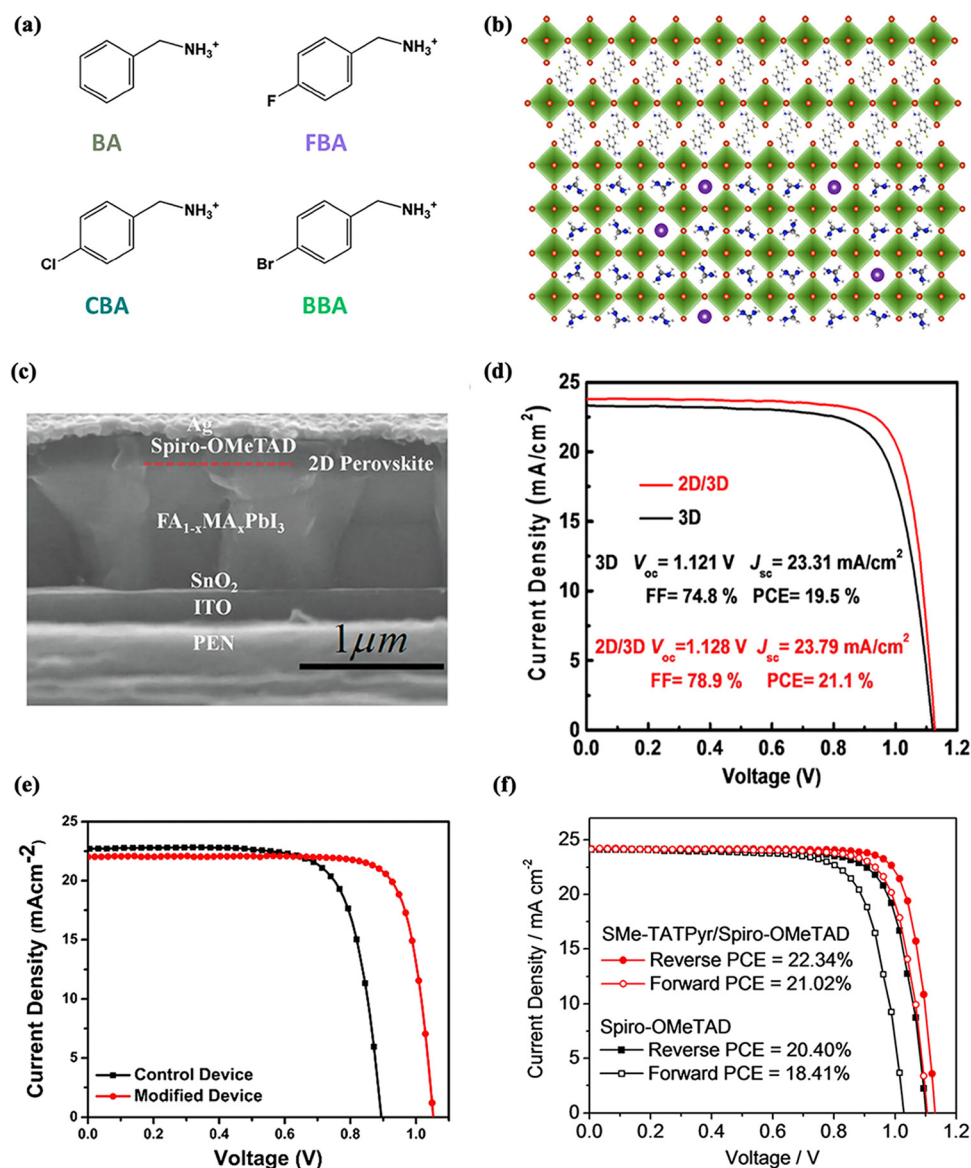

Fig. 11 Two-dimensional (2D) materials for perovskite/HTL interfaces of normal structural PSCs. (a) Schematic diagrams of the structure of BA and its halogenated derivatives (FBA, CBA and BBA) and (b) crystal diagram of the BA-based 2D perovskite layer on 3D perovskite. Reproduced with permission from ref. 116. Copyright 2020 Elsevier. (c) Cross-sectional SEM image and (d) J−V curves of PSCs based on the 2D perovskite structure. Reproduced with permission from ref. 118. Copyright 2021 Wiley. (e) J−V curves of PSCs based on pristine and MoS_2-modified devices. Reproduced with permission from ref. 119. Copyright 2020 Elsevier. (f) J−V curves of PSCs based on Spiro-OMeTAD and Spiro-OMeTAD/SMe-TATPyr. Reproduced with permission from ref. 120. Copyright 2021 Elsevier.

energy loss and carrier recombination at the interface and promoting hole transfer from the perovskite to the HTL. The flexible PSCs prepared after the modification achieved an outstanding efficiency of 21.1% with a certified PCE of 20.5% (Fig. 11c and d). Notably, the device showed enhanced long-term stability due to the supportive impact of the 2D perovskite layer on the underlying 3D perovskite.

In 2020, 2D-MoS_2 was applied to the perovskite/HTL interface.[119] Insertion of this material as an interfacial layer can regulate the energy-level alignment of the HTL and the perovskite, which can suppress interfacial charge accumulation and increase the charge extraction rate. Moreover, the defect state was reduced, and the degradation of the active layer was improved. Ultimately, the efficiency of the device structure based on $FTO/c-TiO_2/SnO_2$ $QD/Cs_{0.1}FAPbI_{3(0.81)}$ $(MAPbBr_{3(0.09)})/MoS_2/PTAA/Au$ reached an efficiency of 18.54% compared with 15.05% for the control device without the MoS_2 layer (Fig. 11e).

Recent studies have shown that sulfur atoms can act as Lewis bases and thus effectively passivate uncoordinated Pb^{2+} deficiencies in perovskites. With this in mind, Li *et al.* designed and synthesized a class of sulfur-rich 2D conjugated small molecules (SMe-TATPyr).[120] After introducing an ultrathin layer of SMe-TATPyr between the perovskite layer and the HTL, they found that SMe-TATPyr matched better with the valence band of the perovskite, so it can effectively reduce the energy loss and improve the V_{oc} of the device. Simultaneously, the S atoms in SMe-TATPyr can passivate the uncoordinated Pb^{2+} defects in the perovskite through Pb–S interactions, thus reducing the interfacial defect recombination. The PCE of the device increased significantly from 20.4% to 22.3%, and 95% of the initial efficiency was preserved after 1500 h of storage under ambient conditions (Fig. 11f).

3.3.2 Quantum dots (QDs). Similar to interfacial modification at the perovskite/ETL interface, QDs applied to the perovskite/HTL interface can also improve the device stability in addition to passivating defects. Inorganic $CsPbBr_{1.85}I_{1.15}$ perovskite quantum-dots (PQDs) were spin-coated onto the perovskite surface as an interface layer.[121] PQDs passivated traps at the interface and grain boundaries and inhibited charge recombination without affecting the phase composition and crystal structure of the perovskite films (Fig. 12a and b). The optimized device achieved an efficiency of 21.14% with a V_{oc} of 1.14 V. More importantly, the test results of subjecting the unencapsulated PSCs to an ambient relative humidity of 40–50% and continuous illumination conditions showed excellent long-term stability. Unlike the single-use of PQDs as an interfacial passivation layer for PSCs, Zheng *et al.* explored their application as surface ligand-carrying carriers.[122] They found that PQDs can fill defective sites on one hand, and on the other hand the organic ligands from the QD synthesis process were separated from the QDs and self-assembled on the surface of the perovskite films, making them hydrophobic and thus preventing the infiltration of water. The study indicated that an $MAPbI_3$ device modified with $CsPbBrCl_2$ QDs obtained a PCE of up to 21.5% and maintained 80% of the initial PCE after 500 hours of continuous light exposure, which presents a novel approach to solving the problems encountered in the preparation of thin films as well as devices. Spiro-OMe TAD is the most commonly used hole transport material for the preparation of high-efficiency PSCs;
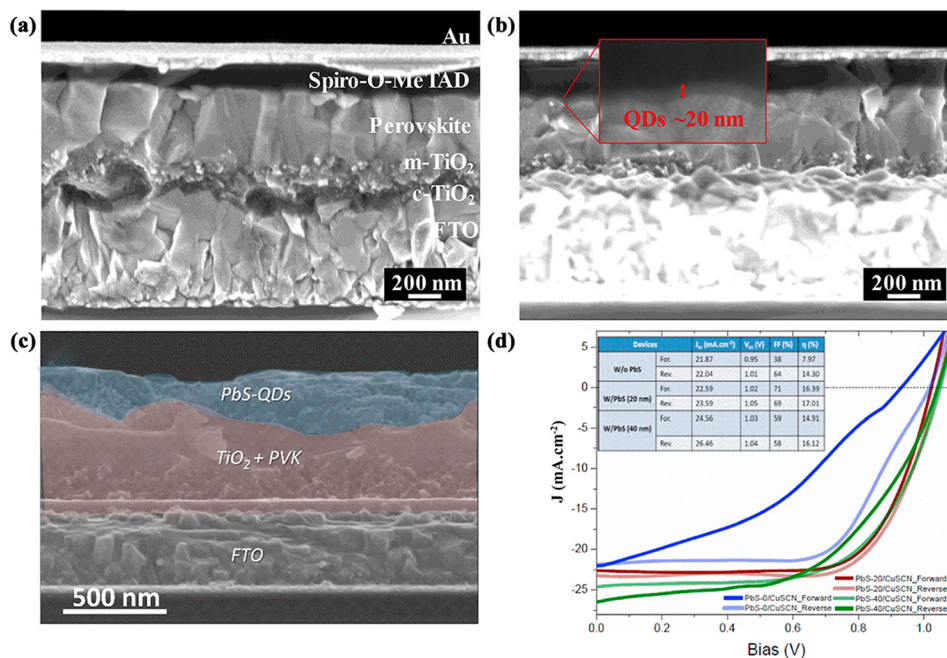

Fig. 12 Quantum dots (QDs) for perovskite/HTL interfaces of normal structural PSCs. Cross-sectional SEM images of PSCs based on (a) an unmodified perovskite surface and (b) the perovskite layer modified with PQDs. Reproduced with permission from ref. 121. Copyright 2019 Elsevier. (c) Cross-sectional SEM image of PSC modified with PbS-QDs, and (d) J–V curves of pristine and PbS-QD-modified PSCs. Reproduced with permission from ref. 127. Copyright 2021 Elsevier.

however, using corrosive 4-*tert*-butylpyridine and the hygroscopic Li-TFSI as indispensable dopants leads to poor device stability.[123,124] To explore modification materials that can replace dopants, in 2021, Cheng *et al.* designed PQDs as a modification layer between the perovskite layer and the dopant-free organic-HTL (o-HTL), which significantly improved the performance of PSCs.[125] The introduction of PQDs not only passivated the defects on the perovskite surface but also optimized the energy-level arrangement at the perovskite/HTL interface. More importantly, PQDs improved the hole mobility by controlling the crystal orientation of various dopant-free o-HTLs. The experimental results indicated that the performance of the PQD-modified and undoped o-HTL-based PSCs can completely replace or even surpass the role of Li$^+$ doping. In particular, the stability of the modified dopant-free PSCs was significantly improved.

PbS-QDs with a broad light absorption and outstanding hole transport ability have also been employed and investigated between the perovskite layer and the HTL. The valence band of PbS-QDs is in the range of $-(5.0$ to $5.1)$ eV, which matches the valence band of MAPbI$_3$. Zhu *et al.* synthesized lead sulfide QDs and dynamically spin coated them onto perovskite films using the reported method.[126] The incorporation of PbS-QDs enhanced the hole extraction rate and reduced carrier recombination. Furthermore, the morphology of the perovskite film is significantly improved as a result. Ultimately, the device obtained a PCE of 19.24%, which was better than that of the unmodified device. Similarly, Ka *et al.* reported the application of PbS-QDs as an interface modification layer for the HTL and the perovskite/HTL interface, respectively, where CuSCN was used as the HTL material instead of the expensive organic HTL.[127] The PbS-QDs were grown directly on the perovskite films using physical deposition, and two devices were subsequently prepared. They found that the PbS-QDs provided a beneficial passivation effect on the perovskite films, enabling better charge separation and collection. The experimental results demonstrated that PbS-QDs exhibited the best performance of 17% when used as an intermediate layer between the perovskite and the CuSCN films (Fig. 12c and d). In particular, the presence of PbS-QDs greatly improved the stability of the device and avoided hysteresis effects.

3.3.3 Small organic molecules and ammonium salts. Similar to modification of the ETL/perovskite interface, organic materials have also been intensively explored for interfacial modification of the perovskite/HTL to passivate imperfections and adjust the surface potential of the perovskite while inducing the formation of physical overlays to enhance the stability. Examples include organic molecules containing electron lone-pair donors and organic ammonium salts.

As mentioned earlier, CuSCN has commonly been considered by researchers as a replacement for expensive organic materials such as spiro-OMeTAD due to its low cost and superior hole mobility and stability, but devices prepared using CuSCN often suffer from V_{oc} loss.[128] Based on this, organic functional molecules were added to the surface of the perovskite layer to passivate imperfections and improve interfacial contacts.[129] The researchers looked for potential functional groups with a high

CuSCN-binding affinity among several pyridine derivatives and found the best functional molecules that bind to both perovskite and CuSCN (Fig. 13a). Ultimately, CuSCN-based devices were prepared using a mixture of 3-pyridyl isothiocyanate (Pr-ITC) and phenylene-1,4-diisothiocyanate (Ph-DITC) as the interfacial modification material and achieved an average PCE of 18.57%, which was very close to that of spiro-OMeTAD-based PSCs.

To improve the FF of PSCs during operation, Wang *et al.* synthesized three carbazole-based fluorinated small molecules, that is, F$_3$BnCz, F$_5$BnCz and F$_4$BnCz$_2$, and explored their effects on the perovskite/HTL interfaces (Fig. 13b).[130] It was investigated that the use of these organic molecules as interfacial layers not only effectively prevented electron transport through holes in the material but also formed an improved contact between the perovskite and the HTL. As a result, the FF was increased from 75% to 80% without affecting the J_{sc} and V_{oc} values, leading to an increase in the PCE from 18.99% to a maximum of 19.96%. In particular, the modified PSCs demonstrated high long-term stability due to the addition of fluorine atoms that make the interfacial layer highly hydrophobic.

Bearing in mind that interfacial organic molecular engineering has been unsatisfactory in improving the lifetime of PSCs, an interfacial engineering strategy using multifunctional ligands was reported, demonstrating that 2,5-thiophenanthrene carboxylic acid ligands can effectively passivate interfacial defects and significantly improve the stability of PSCs.[131] This modification was ascribed to the interaction between the ligand and the perovskite layer at the nanomolecular/sub-nanomolecular level. This ligand improved various defects, inhibited interfacial reorganization, and reduced ion migration in multiple ways.

Most of the organic molecules used to passivate interfacial defects create an electrically insulating layer at the interface that hinders charge extraction. Zhao *et al.* introduced an interfacial engineering strategy using the highly crystalline small molecule 2,7-dioctyl[1]benzothieno[3,2-*b*][1]benzothiophene (C8-BTBT) (Fig. 13c). C8-BTBT interacts with the perovskite surface, thus reducing the interfacial defects.[132] In addition, this strategy stabilized the interface by reducing the electrically insulating aggregates. Ultimately, the absolute efficiency of the C8-BTBT-modified device was increased by more than 2% and the heat resistance of the spiro-OMeTAD layer resulted in a significant improvement.

Also to solve this drawback, researchers explored the possibility of 2-(3′′′,4′-dimethyl-[2,2′:5′,1′′:5′′,2′′′-quaterthiophen]-5-yl)ethan-1-ammonium iodide (4Tm) to modify the perovskite/HTL interface.[133] It was found that the 4Tm molecular layer and the thin 2D perovskite (4Tm)$_2$PbI$_4$ layer combined to form a multifunctional capping layer (MCL) as a conjugated ligand between the perovskite and the HTL. This promoted charge transfer throughout the device by improving the energy-level alignment and stabilized the perovskite interface and lattice by inhibiting ion migration to reduce interfacial non-radiative recombination (Fig. 13d). The PCE of the MCL-based modified PSC was improved to 22.06% with long-term operational stability.

Currently, the passivation mechanism of most organic ammonium salts such as PEAI works by reacting with ions

13628 | *J. Mater. Chem. C*, 2022, **10**, 13611–13645

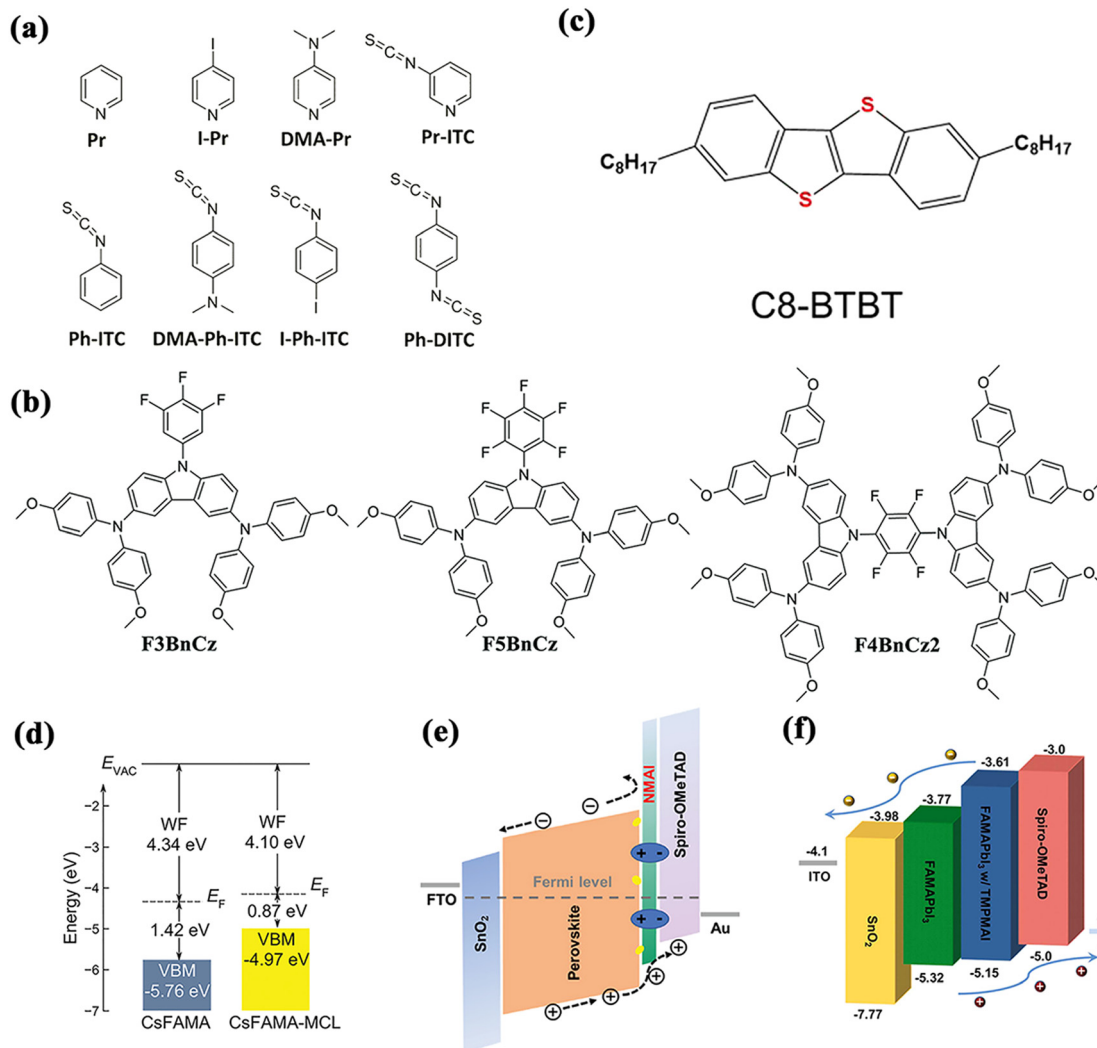This journal is © The Royal Society of Chemistry 2022

Fig. 13   (a)–(c) Structure diagrams of various organic molecules used to modify the perovskite/HTL interface of normal structural PSCs. (a) Reproduced with permission from ref. 129. Copyright 2019 The Royal Society of Chemistry. (b) Reproduced with permission from ref. 130. Copyright 2020 The Royal Society of Chemistry. (c) Reproduced with permission from ref. 132. Copyright 2021 American Chemical Society. (d) Energy level diagram of PSCs based on MCL. Reproduced with permission from ref. 133. Copyright 2021 Wiley. (e) Energy level diagram of PSCs based on NMAI. Reproduced with permission from ref. 136. Copyright 2020 Wiley. (f) Energy level diagram of PSCs based on TMPMAI. Reproduced with permission from ref. 138. Copyright 2022 Elsevier.

not bound to ligands or *via* the formation of a low-dimensional perovskite phase. For instance, cetyltrimethylammonium bromide (CTAB) was applied to the surface of the perovskite layer and subjected to a simple post-treatment.[134] Two useful effects here were that the ammonium group in CTAB may anchor to the MAPbI$_3$ film surface to passivate defects, and that the moisture stability was improved through the attachment of long carbon chains at the perovskite surface. The experimental results indicated that the champion photovoltaic performance of 18.95% and the steady-state output PCE of 18.11% were obtained by modifying the optimal CTAB concentration. Specifically, the CTAB-treated MAPbI$_3$ device exhibited better operating stability than the control device under the same conditions.

Considering the importance of improving the thermal stability of PSCs, Salado *et al.* explored the effect of three different

substituted thiazolium iodide (TMI) salts on the perovskite/HTL interface.[135] Not only can TMI control the possible recombination paths at the perovskite/HTL interface but it can also reduce the density of shallow and deep traps due to the passivation of iodide vacancies in the lattice, thus increasing both V_{oc} and FF. More importantly, unencapsulated devices utilizing TMI exhibited outstanding intrinsic and thermal stability due to the interaction between the thiazole salt and the perovskite surface.

In contrast to previous reports, Liang *et al.* investigated the interfacial modification of 1-naphthylmethylamine iodide (NMAI) and demonstrated an alternative passivation mechanism, namely chemical passivation.[136] The NMAI, with a high formation energy, left NMA$^+$ functional groups on the surface of the perovskite film, thus effectively inhibiting defect recombination. Simultaneously, the charge accumulation was controlled by

inducing energy-level bending, which improved the minority carrier recombination due to charge blockage (Fig. 13e). The final prepared device revealed an efficiency of 21.04% and a V_{oc} of up to 1.20 V as well as long-term stability.

Another unique strategy uses (Me-PDA)Pb$_2$I$_6$, which can form 3D 'perovskitoid' structures instead of a low-dimensional perovskite.[137] This interfacial layer was induced to form a thin 3D perovskite-like structure acting at the perovskite/HTL interface. Compared with the commonly used 2D structure of (PEA)$_2$PbI$_4$, the device derived using (Me-PDA)Pb$_2$I$_6$ was characterized by a superior film quality, a longer carrier lifetime and a higher carrier mobility, together with a lower surface defect density. The device efficiency was thus significantly improved to 22.0% with long-term operational stability.

In 2022, a new organic ammonium salt, namely *N,N,N*-trimethyl phenylmethyl ammonium iodide (TMPMAI), was successfully designed and applied at the perovskite/HTL interface.[138] This strategy not only passivated interfacial defects (mainly targeting Pb^{2+} as a deep defect in the perovskite) *via* interaction of the introduced benzene ring with the perovskite but also created a gradient energy distribution at the interfaces, thus effectively suppressing non-radiative recombination (Fig. 13f). Ultimately, the device based on TMPMAI modification obtained an outstanding PCE of 23.1% with long-term stability.

3.3.4 Other interface-modification materials. Besides the above interfacial treatment strategies, other creative approaches

are being investigated and reported. For example, NiO$_x$ was introduced into the interface between the perovskite and the HTL.[139] The NiO$_x$ layer was spin-coated on top of the perovskite layer, which not only became a part of the HTL but also acted as an interface modification layer to reduce the interfacial defect density of the perovskite. The device incorporating the NiO$_x$ layer achieved stronger carrier extraction and a better-matched energy-level alignment, resulting in a champion PCE of 21.66%. In addition, the NiO$_x$/spiro-OMeTAD bilayer device had an enhanced stability such that an initial efficiency of 90% for over 1200 hours could be maintained (Fig. 14a and b).

A passivation strategy for the perovskite/HTL interface using potassium acetate (K-Ac) was presented.[140] The unique K-Ac can be soluble in a wide range of solvents, enabling it to be used as a bottom and top interface layer. In n–i–p devices, this interfacial passivation layer improved the energy-band alignment of the perovskite/HTL interface, ultimately achieving a superior efficiency of 21.57% compared with the control devices. In particular, the potassium passivation layer in the inverted device changed the orientation of the perovskite particles and improved the charge transport, which also resulted in a more outstanding optoelectronic performance (Fig. 14c and d). The generalizability of this passivation strategy deserves continued attention from researchers.

In addition, other interface-modification techniques have been used to deposit the modification materials at the perovskite/HTL

Fig. 14 *J–V* curves (a) and stability curves (b) for the perovskite/HTL interfaces of normal structural PSCs based on pristine and NiO$_x$-modified interfaces. Reproduced with permission from ref. 139. Copyright 2019 American Chemical Society. *J–V* curves for n–i–p (c) and p–i–n (d) structures of normal structural PSCs based on pristine and K-Ac-modified interfaces. Reproduced with permission from ref. 140. Copyright 2021 Wiley.

interface. All of these approaches showed promise and significant advantages for the commercial application of PSCs, although the process often requires significant time. Typical modification materials that can enhance both the device performance and the stability in the above interfaces are screened and summarized in Table 2.

3.4 Dual interfacial modification engineering

In recent years, there has been an increasing number of researchers exploring the novel strategy of simultaneously modifying the ETL/perovskite and perovskite/HTL dual interfaces in order to improve the device performance more comprehensively. Either the same material is applied or different materials are modified separately, with similar approaches as described in the previous section. For example, organic cationic-based n-BAI compounds were induced to form 2D perovskite layers as double-side passivation layers.[141] It was found that the double-side-modified layer effectively suppressed the non-radiative recombination on both sides of the active layer. The discontinuity of the passivation layer remained unaffected by the conductive channel between the perovskite and the CTL to the extent that effective charge extraction was maintained (Fig. 15a and b). The modified device revealed one

of the highest V_{oc} values of 1.20 V and a PCE of 22.60% with negligible photocurrent hysteresis.

Such modification has also been made for QDs. Chen *et al.* applied $Ti_3C_2T_x$ quantum dots (TQDs) to both the ETL and perovskite layers, and, in particular, they also explored the doping effect of $Cu_{1.8}S$ nanoparticles on the HTL – thus it can be called a triple interfacial modification.[142] On the one hand, TQDs in mesoporous titania reduced the interfacial defects, improving the electron transport in the ETL/perovskite. On the other hand, the TQDs located in the perovskite/HTL increased the crystallite size and conductivity of the perovskite by passivating the recombination centers of charge, thus charge separation and transport were significantly promoted (Fig. 15c and d). Furthermore, the HTL with the incorporation of $Cu_{1.8}S$ showed a higher hole mobility and conductivity as well as a better film quality, and also slowed down the decomposition of the perovskite. This resulted in PSCs with multiple interfacial modifications with TQDs and $Cu_{1.8}S$ nanoparticles, reaching a PCE of 21.64%.

Similarly, WO_x is an n-type transition metal semiconductor oxide with a wide bandgap and a high electron mobility, which has been commonly employed in photocatalysts, electrochromic materials, optical devices, *etc.*[77] WO_x nanorods doped with europium ions (Eu-WO_x) were also introduced into both

Table 2 Modification materials at the perovskite/HTL interface with the ability to simultaneously improve the efficiency and stability of normal structured PSCs

Modification materials		Perovskite	Main roles	PCE [%]	Stability	Ref.
Two-dimensional materials	CF_3PEAI	$FA_{1-x}MA_xPbI_3$	Reduce energy loss and carrier recombination at the interface	20.5	Over 86% of initial efficiency after 880 h of aging	118
	SMe-TATPyr	$FA_{1-x}MA_xPbI_3$	Reduce energy loss and interface defect recombination	22.3	95% initial efficiency for 1500 h of storage under ambient conditions	120
Quantum dots (QDs)	PQDs ($CsPbBrCl_2$)	$CsPbBr_{1.85}I_{1.15}$	Fill defective sites, inhibit water penetration	21.5	80% of initial efficiency after 500 h of continuous light exposure	122
	PbS-QDs	$MAPbI_{3-x-y}Cl_xBr_y$	Passivate interface defects, improve charge separation and collection	17	Over 84% of initial efficiency under continuous sunlight exposure and storage in ambient air for over 30 d	127
Small organic molecules and ammonium salts	$F4BnCz_2$	$MAPbI_3$	Prevent electrons from transporting material through holes	19.96	80% of initial efficiency for 23 d of storage	130
	2,5-Thiophenanthrene carboxylic acid ligands	$FA_{0.97}MA_{0.03}PbI_{2.91}Br_{0.09}$	Passivate interface defects, improve the stability of PSCs	23.4	87% of initial efficiency after 1440 h	131
	4Tm	$Cs_{0.05}(FA_{0.87}MA_{0.13})_{0.95}Pb(I_{0.87}Br_{0.13})_3$	Improve energy-level alignment, reduce interfacial non-radiative recombination	22.06	85% of maximum efficiency after 700 h	133
	CTAB	$MAPbI_3$	Passivate defects, improve moisture stability	18.11	Over 60% of initial efficiency after 1800 m	134
	TMI	$MAPbI_3$	Control the possible reorganization paths on the interface, reduce the trap density	18.93	95% of initial efficiency after 800 h	135
	NMAI	$Cs_{0.05}(MA_{0.15}FA_{0.85})_{0.95}Pb(I_{0.85}Br_{0.15})_3$	Suppress defects and minority carrier recombination	21.04	98.9% of the initial efficiency after 3240 h	136
	$(Me-PDA)Pb_2I_6$	$(FAPbI_3)_{0.85}(MAPbI_2Br)_{0.10}(CsPbI_3)_{0.05}$	Improve film quality, carrier lifetime and carrier mobility, reduce surface defect density	22.0	90% of the initial efficiency after 1008 h	137
	TMPMAI	$FAMAPbI_3$	Passivate interfacial defects, inhibit non-radiative recombination	23.1	Maintain initial efficiency after 96 d	138
Other interface modification methods	NiO_x	$(FAPbI_3)_x(MAPbBr_3)_{1-x}$	Reduce interfacial defect density, improve carrier extraction capability and energy-level alignment	21.66	90% initial efficiency for 1200 h	139

This journal is © The Royal Society of Chemistry 2022

J. Mater. Chem. C, 2022, **10**, 13611–13645 | **13631**
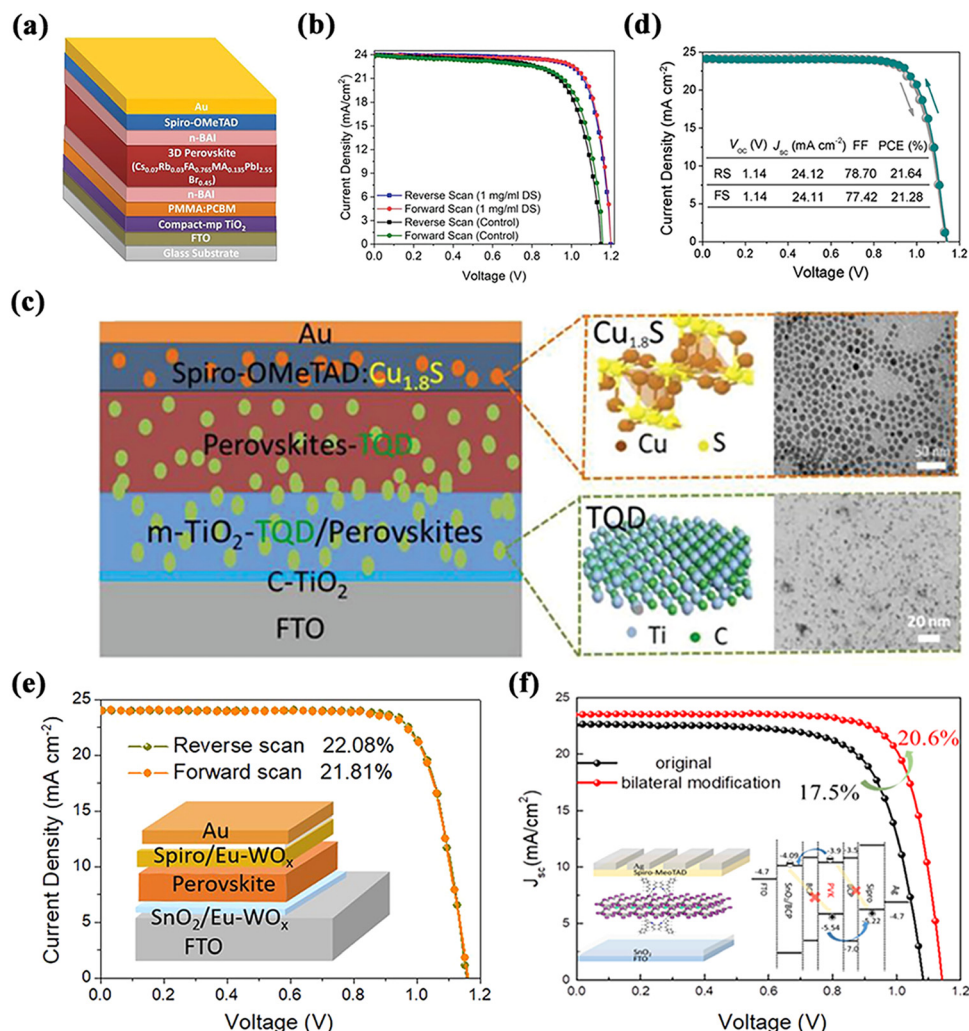
Fig. 15 Schematic diagram of the structure of dual-interface-modified PSCs (a) and $J-V$ curves (b) based on n-BAI. Reproduced with permission from ref. 141. Copyright 2019 Wiley. Modification with TQD and $Cu_{1.8}S$ (c) and $J-V$ curves (d) based on this device architecture. Reproduced with permission from ref. 142. Copyright 2020 Wiley. (e) Structure and $J-V$ curves of dual-interface-modified PSC with Eu-WO$_x$. Reproduced with permission from ref. 143. Copyright 2021 Elsevier. (f) Structure and $J-V$ curves of dual-interface-modified PSC with BCP. Reproduced with permission from ref. 144. Copyright 2021 American Chemical Society.

the ETL and HTL to improve the performance.[143] The modified PSCs obtained a 22.08% hysteresis-free photovoltaic performance and better operational stability (Fig. 15e). This result was attributed to the significant improvement in electrical conductivity, carrier mobility, and crystal quality of the perovskite films by the Eu-WO$_x$ nanorods, as well as the significant improvement in the electron/hole extraction efficiency at the perovskite/ETL and perovskite/HTL interfaces through proper energy-band alignment. Likewise, n-type semiconductor materials (such as BCP) have been used for bi-directional modification studies of PSCs.[144] The films modified with BCP achieved better crystallinity and superior interfacial contact, resulting in high-performance devices with a PCE of 20.6% (Fig. 15f).

AgBiS$_2$ has also been investigated as a modification layer for the ETL/perovskite interface, improving the energy-level alignment and enhancing the charge transport capability.[145] In addition, the researchers avoided the problem of inferior

conductivity by using polyethylene glycol (PEG) in various solvents to modify the perovskite/HTL interfaces instead of adding it directly to the perovskite precursor solution. The grain size and crystallinity of the perovskite films were significantly improved. Consequently, the device modified with the dual interface achieved an efficiency of 21.19% and showed strong UV stability and stability against moisture absorption.

Interestingly, Chen *et al.* developed a guided transfer strategy to achieve the simultaneous modification of the perovskite and ETL films.[146] Firstly, Eu^{3+} was doped into SnO$_2$ to passivate its surface defects, and then Eu^{3+} diffused into the perovskite/ETL interface *via* directional motion. Under the synergistic effect of both, the trap density in the different films was significantly reduced and the electron mobility of the ETL was increased markedly. The experimental results indicated that the obtained PSCs showed a PCE of up to 20.14%. In particular, the unencapsulated PSCs were efficient and slowly

13632 | *J. Mater. Chem. C*, 2022, **10**, 13611–13645

This journal is © The Royal Society of Chemistry 2022

degraded by only 13% after 84 days of storage in an ambient atmosphere.

3.5 Perovskite/top electrode interface

Recent work on the interfacial modification of the top electrode of normal PSCs has largely focused on the interface between the perovskite layer and the carbon electrode. In 2013, Han *et al.* used a carbon electrode as the top electrode of the PSCs and prepared the first fully printed HTL-free PSCs, obtaining a PCE of 6.64%.[49,52] Since then, research into replacing the traditional noble metal with carbon as the top electrode has been gradually developed. However, this device structure has so far suffered from severe performance losses at the back electrode interface, including energy-level mismatch and ineffective hole extraction. Based on this, a 2D perovskite passivation layer was utilized as an electron-blocking layer (EBL) to achieve the purpose of suppressing non-radiative recombination and reducing

interfacial recombination losses (Fig. 16a). The final HTL-free PSCs treated with 2D perovskite interfaces achieved a maximum efficiency of 18.5%, accompanied by enhanced device stability (Fig. 16b).[147] Wu *et al.* utilized a thin layer of poly(ethylene oxide) (PEO) to improve the interfacial energy-level alignment, which was verified through UV emission spectroscopy measurements. Accordingly, a high efficiency value of 14.9% was exhibited. In particular, the modified device retains 77% of its initial PCE after 192 h of storage under unencapsulated dual 85 °C aging conditions (Fig. 16c–e).[148]

In addition to carbon electrodes, PSCs with an efficiency greater than 9% were obtained by applying amorphous indium zinc oxide (IZO) layers *via* sputtering as broadband transparent back electrodes (Fig. 16f and g). When MoO_x was inserted as a buffer layer, the efficiency could be increased to 10.3%.[149] In particular, an efficiency of more than 18% was obtained after applying the modified cells to a four-terminal tandem device.
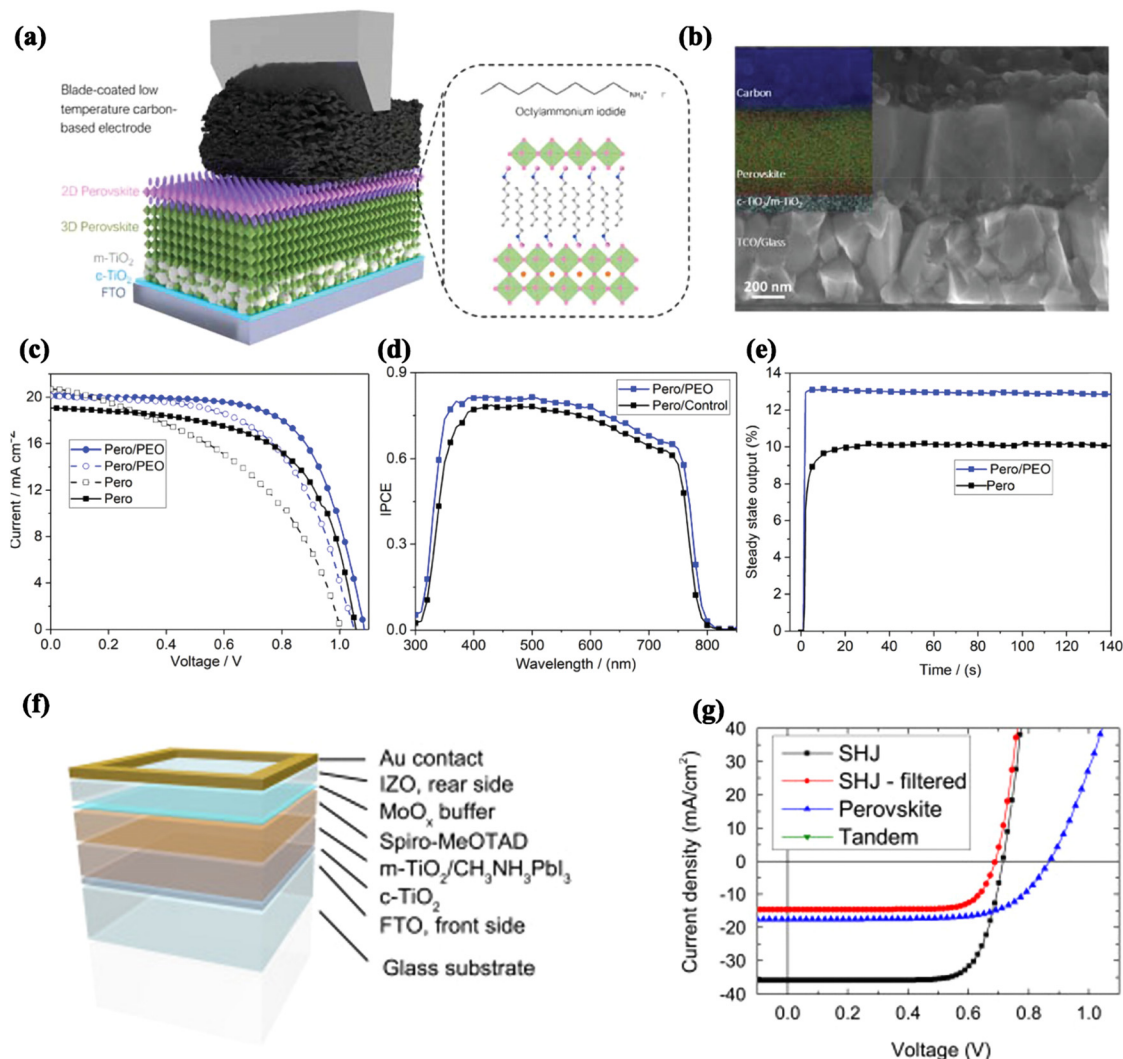

Fig. 16 (a) Schematic diagram and (b) SEM image of the perovskite/top electrode interface of HTM-free C-PSCs based on a 2D perovskite. Reproduced with permission from ref. 147. Copyright 2022 Wiley. (c) *I–V* curves, (d) IPCE curves and (e) steady-state output curves for the perovskite (Pero)/top electrode interface based on PEO. Reproduced with permission from ref. 148. Copyright 2019 Wiley. (f) Schematic diagram of the structure of a typical ST-PSC and (g) *J–V* curves for different device structures based on MoO_x. Reproduced with permission from ref. 149. Copyright 2015 Elsevier.

This journal is © The Royal Society of Chemistry 2022

J. Mater. Chem. C, 2022, **10**, 13611–13645 | **13633**

4. Interfacial engineering in the inverted structure

4.1 Bottom electrode/HTL interface

In PSCs with inverted structures, the acidic nature and electrical inhomogeneity of PEDOT:PSS can negatively affect the chemical stability and electron-blocking ability of the ITO/PEDOT:PSS interface. Some SAMs can be used to solve this problem by modulating the WF of ITO. For example, SAMs containing fluorinated functionalized boronic acid derivatives were investigated for their effectiveness in modifying the ITO surface of planar PSCs.[150] The results after SAM treatment showed that the short-circuit current was enhanced and the trap states of the interface were improved *via* passivation when the WF of ITO was increased. In addition, SAM modification can also be used to protect electrodes that are made of ITO and PEDOT:PSS. Planar PSCs with a 16% efficiency were successfully designed with low hysteresis, high reproducibility, high stability, and high efficiency after SAM modification.

4.2. HTL/perovskite interface

Among inverted and normal PSCs, the main difference lies in the swapping of the ETL and HTL positions and the matching of the functional valence bands after the swapping. Polymer-based hole-transport materials have a relatively high hole mobility and can be easily modified from a molecular perspective, making them ideal for inverted PSCs. The extensively employed poly(3, 4-ethylenedioxythiophene):polystyrene sulfonate (PEDOT:PSS) affects the V_{oc} of the cells due to its energy-level problem, and its acidic aqueous solution is corrosive to ITO glass, which is detrimental to the long-term durability of the PSC.[151,152] Therefore, numerous modification strategies have been explored to address these described defects.

Zhou *et al.* used the multifunctional ionic liquid 1-ethyl-3-methylimidazolium chloride (EMIC) to modify the PEDOT:PSS HTL/perovskite interface, which regulated the interfacial contact between the HTL and the perovskite layer.[153] Furthermore, the crystalline quality of the perovskite film was improved and the charge complex loss was reduced. Notably, they pioneered the replacement of PCBM with the *S*-acetylthiocholine chloride molecule. The efficiency of the finally prepared inverted PSCs reached 20.06% with outstanding stability (Fig. 17a).

Cesium iodide (CsI) was also applied using the interfacial modification strategy by doping into PEDOT:PSS.[154] The material reacts with PbI_2 to form $CsPbI_3$, improving the interfacial contact and charge transport of the PEDOT:PSS/perovskite interface. In addition, the reduction of the WF of the HTL enhanced its hole-transport properties and suppressed non-radiative recombination. The inverted PSCs modified with CsI exhibited an excellent PCE of 20.22% with negligible hysteresis (Fig. 17b). More importantly, a higher V_{oc} of 1.084 V was achieved.

Quasi-2D (Q-2D) perovskite films have been shown to have multiphase structures with different n values (the number of laminated inorganic substances) and to facilitate electron–hole separation.[155] However, Q-2D perovskite materials are still far from being comparable to 3D perovskite materials. Liu *et al.*

found that in inverted PSCs, the deposition of Q-2D perovskite led to the disappearance of this vertical phase distribution. This was mainly attributed to the acidic PEDOT:PSS caused the conversion of perovskite precursors from colloids to solutions. Based on this, they introduced a self-assembly layer of 4-bromobenzenediazonium tetrafluoroborate (BrB), which enabled the Q-2D perovskite films to form the required vertical phase distribution (Fig. 17c). The champion device exhibited a high V_{oc} of 1.11 V and a PCE of 13.74%, as well as superior stability.

Recently, to address the problem of recombination loss due to doping of PEDOT:PSS, aqueous NaOH was used to de-dope the PEDOT:PSS layer and to increase the conductivity by adjusting the thickness of the layer to achieve effective charge transport.[156] The de-doped PEDOT:PSS/perovskite interface demonstrated a significantly lower recombination loss, leading to an increase in the device V_{oc}, FF and PCE. This modification strategy provided a potential direction for the application of PEDOT:PSS in inverted PSCs.

Poly(triarylamine) (PTAA) was introduced into PSCs by Nam Joong Jeon *et al.* to show excellent performance as a hole transport material.[157] Interestingly, the material can also be utilized as an interfacial modification layer to play a role such as defect passivation. Its mechanism of action to reduce interfacial recombination was evidenced through a simulation strategy based on a drift–diffusion model.[158,159]

Although PTAA is currently the preferred material because of its better matching energy levels, higher transport properties, and its ability to significantly improve the long-term stability of the cells, the poor conductivity and surface wettability of PTAA lead to an impaired device performance.[160] Thus, it is crucial to carry out suitable modifications to the PTAA layer. The 3-(1-pyridinio)-1-propanesulfonate (PPS) molecule was designed as a chemical bridge at the PTAA/perovskite interface.[161] The sulfonate in the PPS molecule can form coordination bonds with Pb^{2+} in the perovskite, and pyridine can be chemically coupled with the phenyl group of PTAA through π–π stacking, which synergistically improves the interfacial properties of the PTAA/perovskite interface. Furthermore, PPS molecules can significantly reduce the non-radiative recombination by passivating the surface defects of the perovskite. As a result, the efficiency of the device was increased to 21.7% with negligible hysteresis (Fig. 17d). Similarly, Xu *et al.* tuned the energy levels and surface wettability by removing the alkyl group of PTAA and adding a multifunctional pyridine unit, together with passivation of the interfacial trap.[162] The difficulties of PTAA as the HTL were thus comprehensively solved. The resulting device achieved a PCE of more than 22% with the benefit of the dense and homogeneous perovskite film (Fig. 17e).

Except for the commonly used organic polymer cavity transport materials, inorganic cavity layer materials such as NiO_x, V_2O_5, and CuSCN have also been extensively explored and researched.[163–165] Among them, NiO_x has received more attention due to its stable chemistry and valence band that matches with the halide perovskite absorber layer. With the application of interface modifiers suitable for NiO_x, a number of significant

13634 | *J. Mater. Chem. C*, 2022, **10**, 13611–13645

This journal is © The Royal Society of Chemistry 2022

Fig. 17 $J-V$ curves and stability curves for the HTL/perovskite interface of an inverted structure PSC based on (a) pristine PEDOT:PSS and EMIC-treated PEDOT:PSS. Reproduced with permission from ref. 153. Copyright 2019 Elsevier. (b) $J-V$ curves for the HTL/perovskite interface of an inverted structure PSC based on PEDOT:PSS and PEDOT:PSS/CsI. Reproduced with permission from ref. 154. Copyright 2019 The Royal Society of Chemistry. (c) $J-V$ curves for the HTL/perovskite interface of an inverted structure PSC based on PEDOT:PSS and BrB/PEDOT:PSS. Reproduced with permission from ref. 155. Copyright 2019 Springer Nature. (d) $J-V$ curves for the HTL/perovskite interface of an inverted structure PSC based on PTAA/PVK, PTAA/PVK:PPS, and PTAA/PPS/PVK:PPS. Reproduced with permission from ref. 161. Copyright 2021 American Chemical Society. (e) $J-V$ curves for the HTL/perovskite interface of an inverted structure PSC based on p-PY, m-PY, o-PY and PTAA-2. Reproduced with permission from ref. 162. Copyright 2022 Wiley. (f) $J-V$ curves for the HTL/perovskite interface of an inverted structure PSC based on pristine and different concentrations of CsBr. Reproduced with permission from ref. 168. Copyright 2020 Wiley. (g) $J-V$ curves for the HTL/perovskite interface of an inverted structure PSC based on NiO_x and NiO_x/N719. Reproduced with permission from ref. 169. Copyright 2021 Wiley. (h) $J-V$ curves for the HTL/perovskite interface of an inverted structure PSC based on NiO_x and NiO_x/SaC-100. Reproduced with permission from ref. 170. Copyright 2021 Elsevier. (i) $J-V$ curves for the HTL/perovskite interface of an inverted structure PSC based on NiO and Cu_xS and Al−CuS. Reproduced with permission from ref. 171. Copyright 2021 Wiley.

advances have been made that are accompanied by certified high PCE values.

Alkali chloride was reported to markedly inhibit the inter-facial recombination of NiO_x hole transport layers in inverted PSCs as an interfacial modification layer.[166] This was mainly attributed to the ordering of the perovskite films being tuned by alkali chloride ions, which reduced the defect density and led to a reduction in interfacial recombination. The V_{oc} of the treated devices reached a high of 1.15 eV with the resulting PCE being significantly improved. Potassium salts, such as KI, KSCN and KNO_3, and other inorganic salts worked in a similar way to this material.[167] However, distinct from the inorganic salts mentioned above, Zhang *et al.* highlighted the focus of CsBr for inverted PSCs to alleviate interfacial stresses caused by lattice mismatch.[168] The resulting treated device achieved a certified

efficiency of 19.7% and favorable stability. The optimization of the perovskite/NiO_x HTL interface led to a substantial reduction in the interfacial defect density and obtained the fast extraction/transfer of holes (Fig. 17f). In this work, a new direction is proposed for modification of the NiO_x/perovskite interface. The organometallic dye molecule (N719) with a mesoporous configuration can not only passivate the defects at the HTL/perovskite interface but can also accelerate the carrier transport.[169] The Lewis basic and acidic groups in the N719 molecule applied to both the NiO_x and perovskite surfaces. At the same time, the hole extraction ability of the perovskite was enhanced. The optimized device achieves a PCE of 20.4%, as well as a higher V_{oc} (Fig. 17g). This strategy provides an opportunity for the selection of dye molecules in terms of interfacial modification materials.

This journal is © The Royal Society of Chemistry 2022

J. Mater. Chem. C, 2022, **10**, 13611–13645 | **13635**

The interfacial reaction between Ni^{3+} on the NiO_x surface and the A-site cation salt in the perovskite precursor solution has been systematically investigated.[170] It was concluded that this reaction affects the effective transport of holes and increases the possibility of non-radiative recombination, thus compromising the device performance. In addition, the stability of the device was degraded due to deprotonation of the precursor amine and the oxidation of iodine to interstitial iodine. Based on this, trimethylolpropane tris(2-methyl-1-aziridinepropionate) (SaC-100) was applied as an interfacial modification layer to target this undesirable reaction. SaC-100 can effectively hinder the reaction of Ni^{3+} with MAI and reduce the V_{oc} loss (Fig. 17h). Through surface treatment, they obtained a 20.21% efficiency and long-term stability.

Meanwhile, Al-doped CuS has been reported to be incorporated into inverted PSCs as an efficient inorganic HTL as well as an interfacial modification material, where the role of aluminum was mainly to modulate the energy-band matching of CuS and the perovskite.[171] This method not only optimizes the crystallization process of the perovskite by passivating the interfacial defects but can also be applied as a new HTL for inverted PSCs, rendering sulfide-based materials remarkably promising as HTL materials (Fig. 17i). Typical modification materials were similarly screened and summarized in Table 3.

4.3 Perovskite/ETL interface

In inverted PSCs, the charge separation and transport at the perovskite/ETL interface determine the overall optoelectronic performance of the device. Compared with the large progress made with hole transport materials, the development of electron transport materials has been relatively slow. Electron transport materials commonly used in inverted PSCs include C_{60} and its derivatives and other non-fullerene electron transport materials. So far, PCBMs are the most extensively utilized electron transport materials due to their suitable energy-level matching, low-temperature solution processability, and favorable electron mobility.[172,173]

The chlorinated n-type fused-ring molecule Cl_6SubPc was introduced into the interface between the PEAI-treated 3D/2D perovskite layer and the C_{60} ETL, resulting in a significant

increase in device efficiency from 20.5% to 22%.[174] More importantly, the stability of the device was also significantly improved to the extent that it rivals those of crystalline silicon cells (Fig. 18a). Although PCBM on its own has a high electron transport capacity, it still suffers from a low coverage on the perovskite layers and interfacial recombination. [6,6]-Phenyl-C_{61}-butyric acid-N,N-dimethyl-3-(2-thienyl)propanam ester (PCBB-S-N) was demonstrated to act as an intermediate layer to aid the growth of subsequent PCBM layers, forming a smooth and continuous film.[175,176] Interestingly, PCBB-S-N can also form a bilayer ETL with PCBM. On the one hand, it regulates the energy-band shift between the perovskite layer and the PCBM ETL. On the other hand, PCBB-S-N contains Lewis bases thiophene and amino groups to play a synergistic role by binding to Pb^{2+} as well as forming hydrogen bonds, respectively (Fig. 18b). Thus, the prepared inverted PSCs have a champion photovoltaic performance of 21.08% as well as a more prominent water resistance and thermal stability.

Similarly, a report demonstrated that the n-type organic molecule homologous perylene diimide tetramer (HPDT) can improve the quality of PCBM films and enhance the performance of inverted PSCs.[177] Its suitable energy level and high electron mobility resulted in the suppression of non-radiative recombination (Fig. 18c). The PCE was thus increased to 19.75% with negligible hysteresis.

The doping of PQDs in triple-cation perovskite was studied to improve the device performance and demonstrated its interfacial passivation properties.[178] The presence of PQDs in the anti-solvent avoided lattice distortion of the different components due to their similar crystal structure to the perovskite films, thus optimizing the interfacial defects. Moreover, the high quality of the obtained perovskite films ensured the reduction of non-radiative recombination and the improvement of the carrier transport capacity during the device operation (Fig. 18d). Finally, more than 21% of the PCE was obtained for the devices modified with CPB-QDs. Another material for modifying the perovskite/ETL interface is PbS-QDs.[179] By depositing PbS-QDs on the perovskite, significant passivation of interfacial defects and suppression of non-radiative recombination of carriers were achieved. This was mainly due to

Table 3 Modification materials at the HTL/perovskite interface with the ability to simultaneously improve the efficiency and stability of inverted structure PSCs

| Modification materials	Perovskite	Main roles	PCE [%]	Stability	Ref.
EMIC	$MAPbI_3$	Improve crystalline quality of perovskite films, reduce charge compound loss	20.06	85% of initial efficiency after 35 d of storage in 60% humidity air	153
BrB	$(BA)_2(MA_{0.95}Cs_{0.05})_3Pb_4I_{13}$	Form vertical phase distribution of Q-2D perovskite films	13.74	88% of initial efficiency after 1400 h of storage in air.	155
KCl	CsFAMA	Reduce defect density and interface recombination	20.96	Over 95% of initial performance after 150 d storage in a nitrogen-filled dry box	166
CsBr	$MA_{1-x}FA_xPbI_{3-y}Cl_y$	Reduce defect density, improve extraction/transfer of cavities	19.70	82% of the initial efficiency after 900 h	168
SaC-100	$MAPbI_3$	Reduce V_{oc} loss and non-radiative recombination by hindering the reaction of Ni^{3+} with MAI	20.21	Over 80% and over 85% of initial efficiency in thermal stability tests and light-stability tests	170
Al-doped CuS	$FAPbI_3$	Improve energy-band matching, passivate interfacial defects	12.02	60% of its initial efficiency after 650 h	171
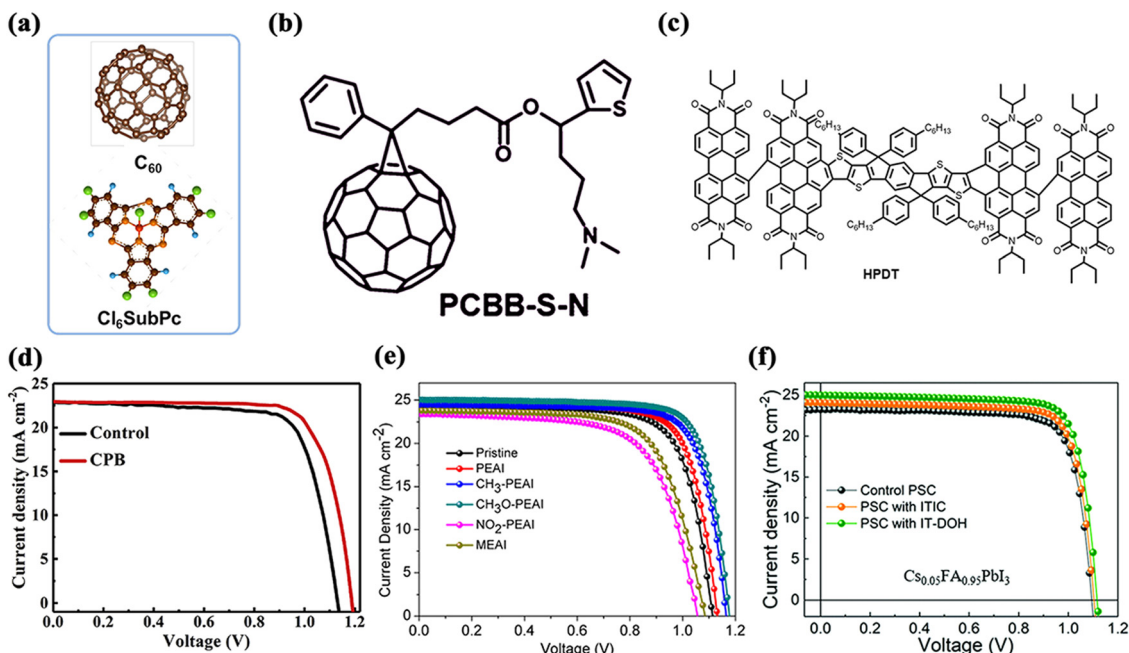
Fig. 18 Structural diagram for the HTL/perovskite interface of inverted structural PSCs based on (a) C_{60} and Cl_6SubPc. Reproduced with permission from ref. 174. Copyright 2021 Elsevier. (b) Structure of PCBB-S-N. Reproduced with permission from ref. 176. Copyright 2019 Wiley. (c) Structure of HPDT. Reproduced with permission from ref. 177. Copyright 2020 Elsevier. (d) *J*–*V* curves based on a pristine device and modification with CPB. Reproduced with permission from ref. 178. Copyright 2020 Elsevier. (e) *J*–*V* curves based on a pristine device and a device with different post-processing. Reproduced with permission from ref. 180. Copyright 2019 American Chemical Society. (f) *J*–*V* curves based on a pristine device and modification with ITIC and IT-DOH. Reproduced with permission from ref. 181 Copyright 2021 The Royal Society of Chemistry.

the suppression of ion-migration phenomena and the acquisition of high-quality PbS-QDs films. The treated inverted PSCs achieved an efficiency of 20.64% as well as a significant improvement in stability.

In addition to Lewis acids/bases and QDs, some ammonium halides have been used to improve the device performance. Zhuang *et al.* systematically investigated the passivation effects of four phenethylammonium iodide (PEAI) compounds that have different substituents.[180] They concluded that the interfacial passivation results were influenced by the electron density of the benzene ring. Among them, phenethylammonium

iodides with electron-donating groups, *i.e.*, methoxy and methyl, can yield excellent passivation. By contrast, phenethylammonium iodides with electron-accepting groups, *i.e.*, nitro, showed poor effects (Fig. 18e). The enhancement of the PCE and stability was attributed to the interaction between the uncoordinated Pb^{2+} and the benzene ring. IT-DOH, a hydroxylated non-fullerene acceptor (NFA) was introduced to modify the perovskite/ETL interface to suppress non-radiative recombination, defects and optimize carrier transport.[181] The unique structure of IT-DOH enabled a more ordered orientation and effective passivation of defects (Fig. 18f). The final experimental results showed

Table 4 Modification materials at the perovskite/ETL interface with the ability to simultaneously improve the efficiency and stability of inverted structure PSCs

Modification materials	Perovskite	Main roles	PCE [%]	Stability	Ref.
Cl_6SubPc	CsFAMA	Passivate interface defects, inhibit halide diffusion	22	98% of initial performance after 2000 h at 80 °C in an inert environment	174
PCBB-S-N	$MAPbI_3$	Regulate energy-band shift, inhibit invading water molecules	21.08	92–95% of initial efficiency after annealing at 85 °C for 500 h at 40–50% ambient atmosphere for nearly 1000 h	175
HPDT	$MAPbI_3$	Improve the quality of PCBM films, inhibit non-radiative recombination	19.75	Maintain a stable efficiency of 19.45%	177
PbS-QDs	$MAPbI_3$	Passivate interfacial defects, inhibit non-radiative recombination	20.64	Maintain a stable efficiency of 20.23%	179
Phenethylammonium iodides with electron-donating groups, *i.e.*, methoxy and methyl	$(FAPbI_3)_{1-x}(MAPbBr_{3-y}Cl_y)_x$	Passivate interface defects	22.98	Maintain almost constant efficiency over 1000 h of storage	180

This journal is © The Royal Society of Chemistry 2022

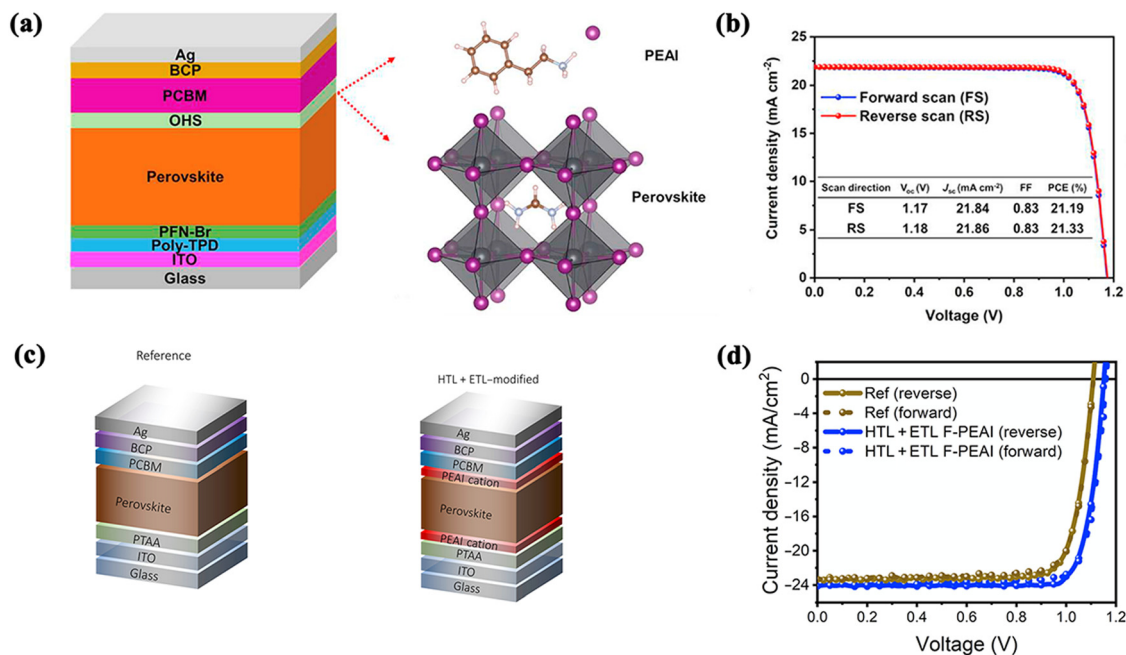*J. Mater. Chem. C*, 2022, **10**, 13611–13645 | **13637**

Fig. 19 Structural diagram of dual-interface-modified PSCs (a) and *J*–*V* curves (b) based on PFN-Br and PEAI. Reproduced with permission from ref. 182. Copyright 2020 Elsevier. Structural diagram of dual-interface-modified PSCs (c) and *J*–*V* curves (d) based on PEAI cations. Reproduced with permission from ref. 184. Copyright 2021 The American Association for the Advancement of Science.

that the NFA-doped devices achieved a champion photovoltaic performance of 22.09% (Table 4).

4.4 Dual-interfacial-modification engineering

The dual-interfacial modification strategy has also attracted extensive attention in inverted PSCs, for example, by depositing PFN-Br and PEAI on the HTL and perovskite layers, respectively, to simultaneously improve the HTL/perovskite interface and perovskite/ETL interface quality, which synergistically brought about the inhibition of non-radiative recombination.[182] The optimized PCE reached a champion value of 21.33% and a stable PCE of 21.01% (Fig. 19a and b).

The application of KSCN for dual interfacial layer treatment has also been reported.[183] Firstly, the passivation effect of K$^+$ is the same as that mentioned above. Then, KSCN can effectively reduce the defect density of the dual surface and inhibit the ion migration through the electrostatic interaction of the perovskite and the strong covalent bonding of NiO$_x$. In addition, the energy-level alignment of the HTL and the perovskite can be optimized. This strategy eventually led to a V_{oc} of 1.14 V and an FF of 0.8 with a champion PCE of 21.23%.

In a recent study, various PEAI-based compounds were used as modified layers at different interfaces.[184] It was proposed that the wettability of the modified HTL/perovskite interface was improved, resulting in more homogeneous films as well as avoiding the generation of nanovoids at the HTL surface. Modification of the perovskite/ETL interface achieved an active passivation effect with the suppression of non-radiative recombination. It is worth mentioning that the joint implementation of both modifications resulted in a simultaneous increase in all the photovoltaic parameters and enabled the easy combination of the ionic liquid with

the perovskite active layer. The final device with a maximum conversion efficiency of 23.7% was obtained (Fig. 19c and d).

4.5 ETL/top electrode interface

The same problem of poor interfacial contact and severe energy loss between the electron transport layer and the metal electrode in inverted PSCs hinders their development. The electrode modification material can adjust the function of the metal electrode, so that the modified low function metal forms an ohmic contact with the ETL to promote electron transport and improve the device performance. A perylene diimide-based zwitterion, QAPDI, has been successfully developed as an interface-modification layer for the ETL/electrode. The material, with its excellent solubility, suitable energy level and high electron mobility, enabled enhanced interfacial contact, a lower energy loss and consequently enhanced electron injection, transport and collection. In particular, the environmental stability was further enhanced by the good hydrophobicity of the modified layer (Fig. 20a).[185] Wang *et al.* inserted a phosphine-inlaid polymer between the top Ag metal electrode and the PCBM.[186] By bonding tightly to the top metal electrode, the modified layer prevented the direct reaction between the electrode and the perovskite, enhancing the rate of electron transfer between the two layers. This study demonstrates that an efficiency of 20.2% can be obtained even in air. It is worth mentioning that the 85 °C aging test further demonstrates that the device can maintain 80% of the initial efficiency for at least 1100 hours (Fig. 20b). The carbolong-derived complexes were also used as the cathode interface layer material for the inverse PSCs, and the results showed that the optimal device FF after modification was as high as 83.52%.[187] The final solar cells were prepared with a 21% (Ag

13638 | *J. Mater. Chem. C*, 2022, **10**, 13611–13645

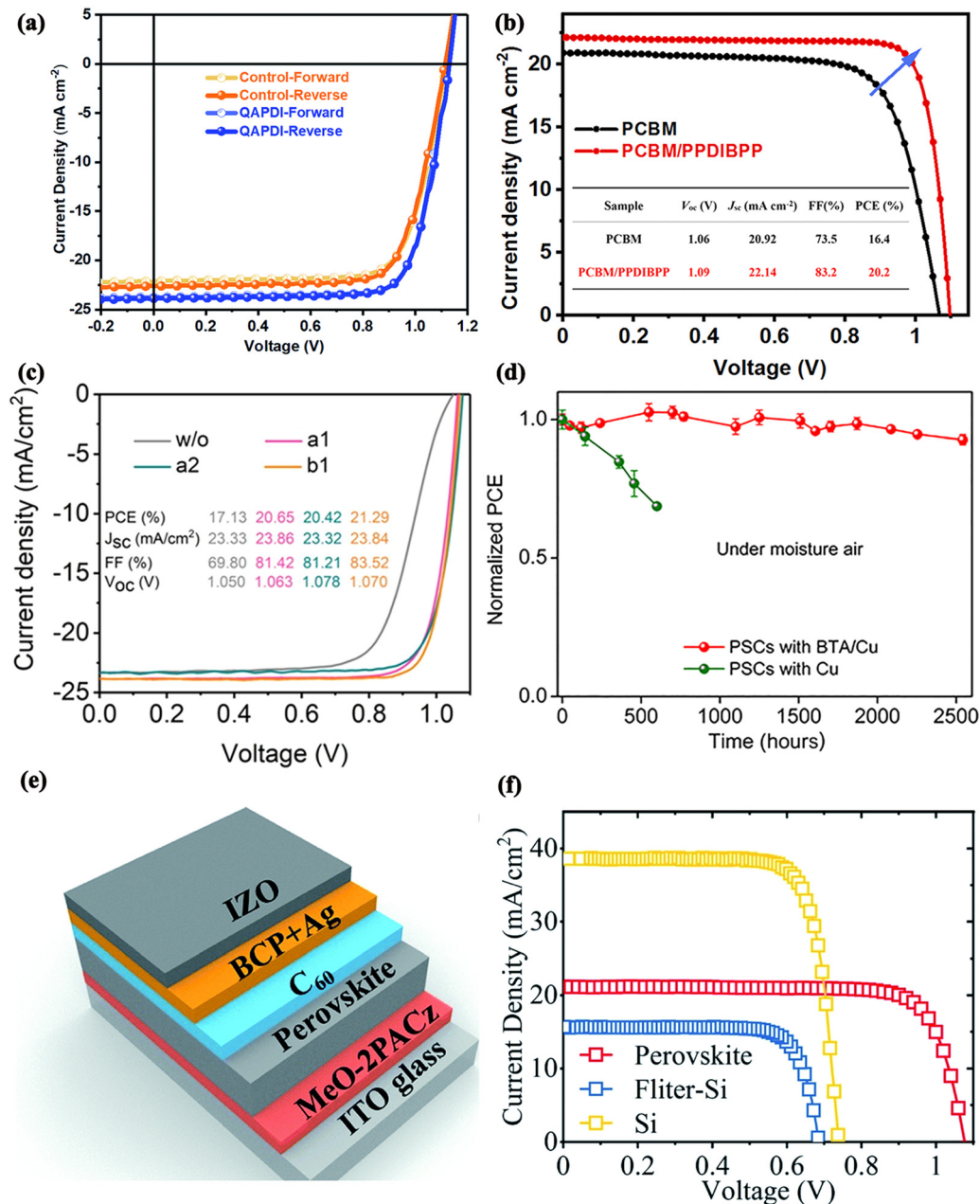This journal is © The Royal Society of Chemistry 2022

Fig. 20 (a) $J-V$ curves for the ETL/top electrode interface of inverted PSCs based on QAPDI. Reproduced with permission from ref. 185 Copyright 2020 The Royal Society of Chemistry. (b) $J-V$ curves for the ETL/top electrode interface of inverted PSCs based on PPDIBPP. Reproduced with permission from ref. 186. Copyright 2021 Elsevier. (c) $J-V$ curves for the ETL/top electrode interface of inverted PSCs based on carbolong-derived complexes. Reproduced with permission from ref. 187. Copyright 2021 American Chemical Society. (d) Stability curves for the ETL/top electrode interface of inverted PSCs based on BTA. Reproduced with permission from ref. 188. Copyright 2020 The American Association for the Advancement of Science. (e) Schematic diagram of the structure of a typical ST-PSC and (f) $J-V$ curves for different device structures based on BCP:Ag. Reproduced with permission from ref. 189 Copyright 2021 The Royal Society of Chemistry.

electrode) and a 20% (Au electrode) photoelectric conversion efficiency (Fig. 20c). The final stability test results proved that the use of carbolong-derived complexes combined with high functional Au electrodes greatly improved the stability of the devices in air and inert gas.

Not to be overlooked, another major challenge for inverted PSCs is the reaction of commonly used metal electrodes with the perovskite layer, leading to electrode corrosion and degradation

of the device performance. Based on this, Fang *et al.* were inspired by metal corrosion protection to improve the stability of devices *via* the introduction of the organic preservative benzotriazole (BTA) before deposition of Cu electrodes.[188] The BTA molecule chemically coordinates with Cu electrodes and forms an insoluble polymer film of [BTA-Cu], which inhibited the electrochemical corrosion and reaction between the perovskite and the Cu electrodes. The devices with the chemical

This journal is © The Royal Society of Chemistry 2022

J. Mater. Chem. C, 2022, **10**, 13611–13645 | **13639**

preservative BTA have an initial PCE of approximately 92.8% after 2500 hours of aging in air (Fig. 20d).

Ying *et al.* applied an interfacial modification strategy to tandem solar cells using a 2,9-dimethyl-4,7-diphenyl-1,10-phenanthroline (BCP):Ag complex to regulate the electrical contact between C_{60} (ETL) and IZO (Fig. 20e).[189] The material not only improves electron transport but also acts as a hole hindrance layer to inhibit charge recombination and has the effect of protecting the C_{60} layer. A final perovskite/silicon four-terminal tandem solar cell with an overall efficiency of 27.59% was achieved (Fig. 20f).

5. Summary and outlook

The multilayer structure of PSCs facilitates the existence of four main interfaces, each of which is directly related to the interfacial carrier dynamics and plays a decisive role in the photovoltaic performance and stability of the devices. Among them, the interfaces of ETL/perovskite, perovskite/HTL, and CTL/electrode are the most critical. Based on these, this Review discusses and summarizes the main research progress for these types of interface engineering. We believe that the main functions of these different interfacial modifications can be summarized as follows: (1) passivation of interfacial defects by filling vacancies or fixing interstitial atoms through chemical interactions of specific functional groups; (2) more rapid charge extraction by modulating the energy-band alignment of neighboring interfacial layers; (3) optimization of the perovskite growth process to assist in the formation of homogeneous, densified, high-performance perovskite films; and (4) improvement of the device stability by blocking external moisture penetration or inhibiting ion migration as a blocking layer.

For the photovoltaic industry, the efficiency, lifetime and cost are considered to be the important indicators of a device's industrial viability. The PSC efficiency has increased dramatically in recent years to the standard point for industrial production, which is no longer the focus of attention. Currently, the maximum lifetime reported for PSCs is at most a few thousand hours, which is far below the lifetime of commercially available photovoltaic devices. Interfacial modification, as a simple and accessible way of optimizing PSCs, not only offers an extremely enhanced effect on the efficiency but also holds significant research potential for making improvements in the PSC lifetime. Interfacial modification is expected to improve the long-term stability of PSCs by isolating water and oxygen and passivating defects, thus attracting increasing attention in recent years, which will be a hot spot for PSC research in the coming years.

In addition, the PCE decreases significantly as the effective area of the PSC is increased, which is limited by the solution-processing method of perovskite films. The efficiency is attributed to the defects in film coverage, the homogeneity and the smoothness of each functional layer that increasingly affect the extraction and transmission of photogenerated carriers as the effective area of the device is enlarged. Therefore, the industrialization of large-area devices for PSCs is a problem that needs to be solved as soon as possible. Future research should focus on the interface-modification methods and materials applicable to large-area devices.

Last but not least, interfacial modification materials need to meet not only the requirements of improving the device performance but also the impact on the operator and the environment. In the future development of PSCs, materials with environmental and recyclable properties, *e.g.*, being biodegradable or naturally degradable, should be developed further. Overall, the interface engineering of PSCs will proceed toward finding effective material systems and processing methods that will completely eradicate defects as well as providing stabilization of the perovskite surface stress. It is predicted that interface engineering will contribute significantly to the future commercialization of PSCs.

Conflicts of interest

There are no conflicts to declare.

Acknowledgements

References

1 S. Wang, X. Wang, B. Liu, Z. Guo, K. K. Ostrikov, L. Wang and W. Huang, *Nanoscale*, 2021, **13**, 17989–18009.

2 J. Cao, X. Lv, P. Zhang, T. T. Chuong, B. Wu, X. Feng, C. Shan, J. Liu and Y. Tang, *Adv. Mater.*, 2018, **30**, 1800568.

3 M. K. Rao, D. N. Sangeetha, M. Selvakumar, Y. N. Sudhakar and M. G. Mahesha, *Sol. Energy*, 2021, **218**, 469–491.

4 S. Wang, Y. Li, X. Wang, G. Zi, C. Zhou, B. Liu, G. Liu, L. Wang and W. Huang, *J. Mater. Sci. Technol.*, 2022, **104**, 155–162.

5 S. Wang, L. Wang and W. Huang, *J. Mater. Chem. A*, 2020, **8**, 24307–24352.

6 S. Wang, B. Liu, X. Wang, Y. Zhang and W. Huang, *Nano Res.*, 2022, **15**, 7026–7033.

7 L. Chao, T. Niu, W. Gao, C. Ran, L. Song, Y. Chen and W. Huang, *Adv. Mater.*, 2021, **33**, 2005410.

8 Z. Sun, X. Chen, Y. He, J. Li, J. Wang, H. Yan and Y. Zhang, *Adv. Energy Mater.*, 2022, **12**, 2200015.

9 K. Yoshikawa, H. Kawasaki, W. Yoshida, T. Irie, K. Konishi, K. Nakano, T. Uto, D. Adachi, M. Kanematsu, H. Uzu and K. Yamamoto, *Nat. Energy*, 2017, **2**, 17032–17040.

13640 | *J. Mater. Chem. C*, 2022, **10**, 13611–13645

This journal is © The Royal Society of Chemistry 2022

10 T. Takamoto1, T. Agui1, A. Yoshida1, K. Nakaido1, H. Juso1, K. Sasaki, K. Nakamora1, H. Yamaguchi1, T. Kodama1, H. Washio1, M. Imaizumi and M. Takahashi, *Sharp Tech. J.*, 2010, **100**, 1–10.

11 Z. Yang, J. Z. Fan, A. H. Proppe, F. P. G. Arquer, D. Rossouw, O. Voznyy, X. Lan, M. Liu, G. Walters, R. Quintero-Bermudez, B. Sun, S. Hoogland, G. A. Botton, S. O. Kelley and E. H. Sargent, *Nat. Commun.*, 2017, **8**, 1325.

12 H. Zhou, Y. Zhang, J. Seifter, S. D. Collins, C. Luo, G. C. Bazan, T. Q. Nguyen and A. J. Heeger, *Adv. Mater.*, 2013, **25**, 1646–1652.

13 A. Kojima, K. Teshima, Y. Shirai and T. Miyasaka, *J. Am. Chem. Soc.*, 2009, **131**, 6050–6051.

14 P. Chen, Y. Bai, M. Lyu, J.-H. Yun, M. Hao and L. Wang, *Sol. RRL*, 2018, **2**, 1700186.

15 J. Gebhardt and A. M. Rappe, *ACS Energy Lett.*, 2017, **2**, 2681–2685.

16 T. M. Brenner, D. A. Egger, L. Kronik, G. Hodes and D. Cahen, *Nat. Rev. Mater.*, 2016, **1**, 15007.

17 T. Miyasaka, A. Kulkarni, G. M. Kim, S. Öz and A. K. Jena, *Adv. Energy Mater.*, 2019, **10**, 1902500.

18 M. Saba, F. Quochi, A. Mura and G. Bongiovanni, *Acc. Chem. Res.*, 2016, **49**, 166–173.

19 A. R. Srimath Kandada and A. Petrozza, *Acc. Chem. Res.*, 2016, **49**, 536–544.

20 H. S. Kim, C. R. Lee, J. H. Im, K. B. Lee, T. Moehl, A. Marchioro, S. J. Moon, R. Humphry-Baker, J. H. Yum, J. E. Moser, M. Gratzel and N. G. Park, *Sci. Rep.*, 2012, **2**, 591.

21 https://www.nrel.gov/pv/cell-efficiency.html.

22 M. R. Filip, S. Hillman, A. A. Haghighirad, H. J. Snaith and F. Giustino, *J. Phys. Chem. Lett.*, 2016, **7**, 2579–2585.

23 N. K. Noel, S. D. Stranks, A. Abate, C. Wehrenfennig, S. Guarnera, A.-A. Haghighirad, A. Sadhanala, G. E. Eperon, S. K. Pathak, M. B. Johnston, A. Petrozza, L. M. Herz and H. J. Snaith, *Energy Environ. Sci.*, 2014, **7**, 3061–3068.

24 G. Volonakis, M. R. Filip, A. A. Haghighirad, N. Sakai, B. Wenger, H. J. Snaith and F. Giustino, *J. Phys. Chem. Lett.*, 2016, **7**, 1254–1259.

25 W. Hui, L. Chao, H. Lu, F. Xia, Q. Wei, Z. Su, T. Niu, L. Tao, B. Du, D. Li, Y. Wang, H. Dong, S. Zuo, B. Li, W. Shi, X. Ran, P. Li, H. Zhang, Z. Wu, C. Ran, L. Song, G. Xing, X. Gao, J. Zhang, Y. Xia, Y. Chen and W. Huang, *Science*, 2021, **371**, 1359–1364.

26 P. Y. Lin, A. Loganathan, I. Raifuku, M. H. Li, Y. Y. Chiu, S. T. Chang, A. Fakharuddin, C. F. Lin, T. F. Guo, L. Schmidt-Mende and P. Chen, *Adv. Energy Mater.*, 2021, **11**, 2100818.

27 K. Wang, W. S. Subhani, Y. Wang, X. Zuo, H. Wang, L. Duan and S. F. Liu, *Adv. Mater.*, 2019, **31**, 1902037.

28 S. Shao and M. A. Loi, *Adv. Mater. Interfaces*, 2019, **7**, 1901469.

29 A. Fakharuddin, L. Schmidt-Mende, G. Garcia-Belmonte, R. Jose and I. Mora-Sero, *Adv. Energy Mater.*, 2017, **7**, 1700623.

30 T. H. Han, S. Tan, J. Xue, L. Meng, J. W. Lee and Y. Yang, *Adv. Mater.*, 2019, **31**, 1803515.

31 Y. Li, H. Xie, E. L. Lim, A. Hagfeldt and D. Bi, *Adv. Energy Mater.*, 2022, **12**, 2102730.

32 W. Yu, X. Sun, M. Xiao, T. Hou, X. Liu, B. Zheng, H. Yu, M. Zhang, Y. Huang and X. Hao, *Nano Res.*, 2021, **15**, 85–103.

33 A. K. Geim, *Science*, 2009, **324**, 1530–1534.

34 K. S. Novoselov, A. K. Geim, S. V. Morozov, D. Jiang, Y. Zhang, S. V. Dubonos, I. V. Grigorieva and A. A. Firsov, *Science*, 2004, **306**, 666–669.

35 M. A. Loi and J. C. Hummelen, *Nat. Mater.*, 2013, **12**, 1087–1089.

36 H. Zhou, Q. Chen, G. Li, S. Luo, T. Song, H. Duan, Z. Hong, J. You, Y. Liu and Y. Yang, *Science*, 2014, **345**, 542–548.

37 J. J. Choi, X. Yang, Z. M. Norman, S. J. Billinge and J. S. Owen, *Nano Lett.*, 2014, **14**, 127–133.

38 Z. Song, S. C. Watthage, A. B. Phillips and M. J. Heben, *J. Photonics Energy*, 2016, **6**, 1947–7988.

39 D. Li, L. Chao, C. Chen, X. Ran, Y. Wang, T. Niu, S. Lv, H. Wu, Y. Xia, C. Ran, L. Song, S. Chen, Y. Chen and W. Huang, *Nano Lett.*, 2020, **20**, 5799–5806.

40 Z. C. Cheng, Y. Y. Fang, A. F. Wang, T. T. Ma, F. Liu, S. Gao, S. H. Yan, Y. Di and T. S. Qin, *J. Cent. South Univ.*, 2021, **28**, 3714–3727.

41 Q. Dong, Y. Yuan, Y. Shao, Y. Fang, Q. Wang and J. Huang, *Energy Environ. Sci.*, 2015, **8**, 2464–2470.

42 P. Schulz, *ACS Energy Lett.*, 2018, **3**, 1287–1293.

43 T. Handa, D. M. Tex, A. Shimazaki, A. Wakamiya and Y. Kanemitsu, *J. Phys. Chem. Lett.*, 2017, **8**, 954–960.

44 V. D'Innocenzo, A. R. Srimath Kandada, M. De Bastiani, M. Gandini and A. Petrozza, *J. Am. Chem. Soc.*, 2014, **136**, 17730–17733.

45 M. Stolterfoht, C. M. Wolff, Y. Amir, A. Paulke, L. Perdigón-Toro, P. Caprioglio and D. Neher, *Energy Environ. Sci.*, 2017, **10**, 1530–1539.

46 Q.-D. Ou, C. Li, Q.-K. Wang, Y.-Q. Li and J.-X. Tang, *Adv. Mater. Interfaces*, 2017, **4**, 1600694.

47 J. W. Lee, S. G. Kim, S. H. Bae, D. K. Lee, O. Lin, Y. Yang and N. G. Park, *Nano Lett.*, 2017, **17**, 4270–4276.

48 I. G. Scheblykin, *Adv. Energy Mater.*, 2020, **10**, 2001724.

49 R. Chen, W. Zhang, X. Guan, H. Raza, S. Zhang, Y. Zhang, P. A. Troshin, S. A. Kuklin, Z. Liu and W. Chen, *Adv. Funct. Mater.*, 2022, **32**, 2200651.

50 C. Ding, L. Yin, L. Zhang, R. Huang, S. Fan, Q. Luo, J. Lin, F. Li, C. Zhao, R. Österbacka and C. Q. Ma, *Adv. Funct. Mater.*, 2021, **31**, 2103820.

51 D. Luo, X. Li, A. Dumont, H. Yu and Z. H. Lu, *Adv. Mater.*, 2021, **33**, 2006004.

52 J. Liu, Q. Zhou, N. K. Thein, L. Tian, D. Jia, E. M. J. Johansson and X. Zhang, *J. Mater. Chem. A*, 2019, **7**, 13777–13786.

53 C. H. Lin, L. Hu, X. Guan, J. Kim, C. Y. Huang, J. K. Huang, S. Singh and T. Wu, *Adv. Mater.*, 2022, **34**, 2108616.

54 B. Chen, S. W. Baek, Y. Hou, E. Aydin, M. De Bastiani, B. Scheffel, A. Proppe, Z. Huang, M. Wei, Y. K. Wang,

This journal is © The Royal Society of Chemistry 2022

J. Mater. Chem. C, 2022, **10**, 13611–13645 | **13641**

E. H. Jung, T. G. Allen, E. Van Kerschaver, F. P. Garcia de Arquer, M. I. Saidaminov, S. Hoogland, S. De Wolf and E. H. Sargent, *Nat. Commun.*, 2020, **11**, 1257.

55 C. Yan, J. Huang, D. Li and G. Li, *Mater. Chem. Front.*, 2021, **5**, 4538–4564.

56 L. Huang, D. Zhang, S. Bu, R. Peng, Q. Wei and Z. Ge, *Adv. Sci.*, 2020, **7**, 1902656.

57 S. Huang, Q. Dong, Y. Shi, L. Duan and L. Wang, *Chem. Eng. J.*, 2020, **394**, 125024.

58 X. Gong, Q. Sun, S. Liu, P. Liao, Y. Shen, C. Gratzel, S. M. Zakeeruddin, M. Gratzel and M. Wang, *Nano Lett.*, 2018, **18**, 3969–3977.

59 S. Wang, T. Sakurai, W. Wen and Y. Qi, *Adv. Mater. Interfaces*, 2018, **5**, 1800260.

60 P. Chen, Z. Wang, S. Wang, M. Lyu, M. Hao, M. Ghasemi, M. Xiao, J.-H. Yun, Y. Bai and L. Wang, *Nano Energy*, 2020, **69**, 104392.

61 L. Tao, J. Qiu, B. Sun, X. Wang, X. Ran, L. Song, W. Shi, Q. Zhong, P. Li, H. Zhang, Y. Xia, P. Müller-Buschbaum and Y. Chen, *J. Energy Chem.*, 2021, **61**, 395–415.

62 L. Yin, Y. Li, X. Yao, Y. Wang, L. Jia, Q. Liu, J. Li, Y. Li and D. He, *Nano Lett.*, 2021, **13**, 96–112.

63 H. Zheng, Y. Wang, B. Niu, R. Ge, Y. Lei, L. Yan, J. Si, P. Zhong and X. Ma, *J. Phys. Chem. C*, 2021, **125**, 15210–15222.

64 K. F. Chen, P. Cai, H. L. Peng, X. G. Xue, Z. M. Wang and L. X. Sun, *J. Cent. South Univ.*, 2021, **28**, 3935–3958.

65 M. Dadashi Firouzjaei, M. Karimiziarani, H. Moradkhani, M. Elliott and B. Anasori, *Mater. Today Adv*, 2022, **13**, 100202.

66 A. Agresti, A. Pazniak, S. Pescetelli, A. Di Vito, D. Rossi, A. Pecchia, M. Auf der Maur, A. Liedl, R. Larciprete, D. V. Kuznetsov, D. Saranin and A. Di Carlo, *Nat. Mater.*, 2019, **18**, 1228–1234.

67 J. Li, T. Jiu, S. Chen, L. Liu, Q. Yao, F. Bi, C. Zhao, Z. Wang, M. Zhao, G. Zhang, Y. Xue, F. Lu and Y. Li, *Nano Lett.*, 2018, **18**, 6941–6947.

68 S. Zhang, H. Si, W. Fan, M. Shi, M. Li, C. Xu, Z. Zhang, Q. Liao, A. Sattar, Z. Kang and Y. Zhang, *Angew. Chem., Int. Ed.*, 2020, **59**, 11573–11582.

69 L. Yao, M. Zhao, L. Liu, S. Chen, J. Wang, C. Zhao, Z. Jia, S. Pang, X. Guo and T. Jiu, *Mater. Chem. Front.*, 2021, **5**, 6913–6922.

70 J. Jimenez-Lopez, B. M. D. Puscher, D. M. Guldi and E. Palomares, *J. Am. Chem. Soc.*, 2020, **142**, 1236–1246.

71 H. Wang, F. Li, P. Wang, R. Sun, W. Ma, M. Chen, W. Miao, D. Liu and T. Wang, *Adv. Energy Mater.*, 2020, **10**, 2000615.

72 C. Tian, K. Lin, J. Lu, W. Feng, P. Song, L. Xie and Z. Wei, *Small Methods*, 2019, **4**, 1900476.

73 T. Wu, C. Zhen, J. Wu, C. Jia, M. Haider, L. Wang, G. Liu and H.-M. Cheng, *Sci. Bull.*, 2019, **64**, 547–552.

74 W. Hui, Y. Yang, Q. Xu, H. Gu, S. Feng, Z. Su, M. Zhang, J. Wang, X. Li, J. Fang, F. Xia, Y. Xia, Y. Chen, X. Gao and W. Huang, *Adv. Mater.*, 2020, **32**, 1906374.

75 Y. Yang, H. Lu, S. Feng, L. Yang, H. Dong, J. Wang, C. Tian, L. Li, H. Lu, J. Jeong, S. M. Zakeeruddin, Y. Liu, M. Grätzel and A. Hagfeldt, *Energy Environ. Sci.*, 2021, **14**, 3447–3454.

76 Z. W. Gao, Y. Wang, H. Liu, J. Sun, J. Kim, Y. Li, B. Xu and W. C. H. Choy, *Adv. Funct. Mater.*, 2021, **31**, 2101438.

77 Y. Hou, C. O. R. Quiroz, S. Scheiner, W. Chen, T. Stubhan, A. Hirsch, M. Halik and C. J. Brabec, *Adv. Energy Mater.*, 2015, **5**, 1501056.

78 F. Ali, C. Roldán-Carmona, M. Sohail and M. K. Nazeeruddin, *Adv. Energy Mater.*, 2020, **10**, 2002989.

79 C. M. Wolff, L. Canil, C. Rehermann, N. Ngoc Linh, F. Zu, M. Ralaiarisoa, P. Caprioglio, L. Fiedler, M. Stolterfoht, S. Kogikoski, Jr., I. Bald, N. Koch, E. L. Unger, T. Dittrich, A. Abate and D. Neher, *ACS Nano*, 2020, **14**, 1445–1456.

80 J. Han, H. Kwon, E. Kim, D.-W. Kim, H. J. Son and D. H. Kim, *J. Mater. Chem. A*, 2020, **8**, 2105–2113.

81 Y. Shi, H. Zhang, X. Tong, X. Hou, F. Li, Y. Du, S. Wang, Q. Zhang, P. Liu and X. Zhao, *Sol. RRL*, 2021, **5**, 2100128.

82 Z. Dai, S. K. Yadavalli, M. Chen, A. Abbaspourtamijani, Y. Qi and N. P. Padture, *Science*, 2021, **372**, 618–622.

83 P. Zhu, S. Gu, X. Luo, Y. Gao, S. Li, J. Zhu and H. Tan, *Adv. Energy Mater.*, 2019, **10**, 1903083.

84 R. Azmi, N. Nurrosyid, S.-H. Lee, M. Al Mubarok, W. Lee, S. Hwang, W. Yin, T. K. Ahn, T.-W. Kim, D. Y. Ryu, Y. R. Do and S.-Y. Jang, *ACS Energy Lett.*, 2020, **5**, 1396–1403.

85 L. Wang, X. Wang, L. Zhu, S.-B. Leng, J. Liang, Y. Zheng, Z. Zhang, Z. Zhang, X. Liu, F. Liu and C.-C. Chen, *Chem. Eng. J.*, 2022, **430**, 132730.

86 Z. Huang, A. H. Proppe, H. Tan, M. I. Saidaminov, F. Tan, A. Mei, C.-S. Tan, M. Wei, Y. Hou, H. Han, S. O. Kelley and E. H. Sargent, *ACS Energy Lett.*, 2019, **4**, 1521–1527.

87 Q. Xiong, C. Wang, Q. Zhou, L. Wang, X. Wang, L. Yang, J. Ding, C. C. Chen, J. Wu, X. Li and P. Gao, *Adv. Funct. Mater.*, 2021, **32**, 2107823.

88 A. A. Zaky, E. Christopoulos, K. Gkini, M. K. Arfanis, L. Sygellou, A. Kaltzoglou, A. Stergiou, N. Tagmatarchis, N. Balis and P. Falaras, *Appl. Catal., B*, 2021, **284**, 119714.

89 H. Xu, Y. Miao, N. Wei, H. Chen, Z. Qin, X. Liu, X. Wang, Y. Qi, T. Zhang and Y. Zhao, *Adv. Energy Mater.*, 2021, **12**, 2103151.

90 H. Bi, B. Liu, D. He, L. Bai, W. Wang, Z. Zang and J. Chen, *Chem. Eng. J.*, 2021, **418**, 129375.

91 C. Zhang, H. Wang, H. Li, Q. Zhuang, C. Gong, X. Hu, W. Cai, S. Zhao, J. Chen and Z. Zang, *J. Energy Chem.*, 2021, **63**, 452–460.

92 M. Fahim, I. Firdous, W. Zhang and W. A. Daoud, *Nano Energy*, 2021, **86**, 106127.

93 P. Finkel, M. G. Cain, T. Mion, M. Staruch, J. Kolacz, S. Mantri, C. Newkirk, K. Kavetsky, J. Thornton, J. Xia, M. Currie, T. Hase, A. Moser, P. Thompson, C. A. Lucas, A. Fitch, J. M. Cairney, S. D. Moss, A. G. A. Nisbet, J. E. Daniels and S. E. Lofland, *Adv. Mater.*, 2022, **34**, 2106827.

94 Y. M. You, W. Q. Liao, D. Zhao, H. Y. Ye, Y. Zhang, Q. Zhou, X. Niu, J. Wang, P. F. Li, D. W. Fu, Z. Wang, S. Gao, K. Yang, J. M. Liu, J. Li, Y. Yan and R. G. Xiong, *Science*, 2017, **357**, 306–309.

95 S. Sonmezoglu and S. Akin, *Nano Energy*, 2020, **76**, 105127.

96 Y. Sun, J. Zhang, H. Yu, J. Wang, C. Huang and J. Huang, *Chem. Eng. J.*, 2021, **420**, 129579.

13642 | *J. Mater. Chem. C*, 2022, **10**, 13611–13645

This journal is © The Royal Society of Chemistry 2022

97 Y. Yang, *ACS Nano*, 2021, **15**, 18679–18682.

98 Q. Lou, Y. Han, C. Liu, K. Zheng, J. Zhang, X. Chen, Q. Du, C. Chen and Z. Ge, *Adv. Energy Mater.*, 2021, **4**, 2101416.

99 J. Tao, X. Liu, J. Shen, H. Wang, J. Xue, C. Su, H. Guo, G. Fu, W. Kong and S. Yang, *Chem. Eng. J.*, 2022, **430**, 132683.

100 X. Zuo, B. Kim, B. Liu, D. He, L. Bai, W. Wang, C. Xu, Q. Song, C. Jia, Z. Zang, D. Lee, X. Li and J. Chen, *Chem. Eng. J.*, 2022, **431**, 133209.

101 D. Liu, H. Zheng, Y. Wang, L. Ji, H. Chen, W. Yang, L. Chen, Z. Chen and S. Li, *Chem. Eng. J.*, 2020, **396**, 125010.

102 H. Liang, Y. C. Hu, Y. Tao, B. Wu, Y. Wu and J. Cao, *ACS Appl. Mater. Interfaces*, 2019, **11**, 43116–43121.

103 M. Tai, X. Zhao, H. Shen, Y. Guo, M. Zhang, Y. Zhou, X. Li, Z. Yao, X. Yin, J. Han, X. Li and H. Lin, *Chem. Eng. J.*, 2019, **361**, 60–66.

104 D. Zhang, X. Zhang, S. Bai, C. Liu, Z. Li, W. Guo and F. Gao, *Sol. RRL*, 2019, **3**, 1900154.

105 S. Tsarev, S. Olthof, A. G. Boldyreva, S. M. Aldoshin, K. J. Stevenson and P. A. Troshin, *Nano Energy*, 2021, **83**, 105774.

106 Z. Xiong, X. Chen, B. Zhang, G. O. Odunmbaku, Z. Ou, B. Guo, K. Yang, Z. Kan, S. Lu, S. Chen, N. A. N. Ouedraogo, Y. Cho, C. Yang, J. Chen and K. Sun, *Adv. Mater.*, 2021, **34**, 2106118.

107 S. You, H. Zeng, Z. Ku, X. Wang, Z. Wang, Y. Rong, Y. Zhao, X. Zheng, L. Luo, L. Li, S. Zhang, M. Li, X. Gao and X. Li, *Adv. Mater.*, 2020, **32**, 2003990.

108 Z. Xiong, L. Lan, Y. Wang, C. Lu, S. Qin, S. Chen, L. Zhou, C. Zhu, S. Li, L. Meng, K. Sun and Y. Li, *ACS Energy Lett.*, 2021, **6**, 3824–3830.

109 J. Luo, F. Lin, J. Xia, H. Yang, R. Zhang, H. A. Malik, H. Shu, Z. Wan, K. Han, R. Wang, X. Yao and C. Jia, *Nano Energy*, 2021, **82**, 105751.

110 W. Ke, P. Priyanka, S. Vegiraju, C. C. Stoumpos, I. Spanopoulos, C. M. M. Soe, T. J. Marks, M. C. Chen and M. G. Kanatzidis, *J. Am. Chem. Soc.*, 2018, **140**, 388–393.

111 C. Xiao, F. Zhang, Z. Li, S. P. Harvey, X. Chen, K. Wang, C.-S. Jiang, K. Zhu and M. Al-Jassim, *Matter*, 2020, **2**, 261–272.

112 C. Liu, X. Zhou, S. Chen, X. Zhao, S. Dai and B. Xu, *Adv. Sci.*, 2019, **6**, 1801169.

113 L. Calió, D. S. Kazim, P. M. Grätzel and D. S. Ahmad, *Angew. Chem.*, 2016, **55**, 14522–14545.

114 M. E. F. Bouduban, V. I. E. Queloz, V. M. Caselli, K. T. Cho, A. R. Kirmani, S. Paek, C. Roldan-Carmona, L. J. Richter, J. E. Moser, T. J. Savenije, M. K. Nazeeruddin and G. Grancini, *J. Phys. Chem. Lett.*, 2019, **10**, 5713–5720.

115 H. Kim, S. U. Lee, D. Y. Lee, M. J. Paik, H. Na, J. Lee and S. I. Seok, *Adv. Energy Mater.*, 2019, **9**, 1902740.

116 G. Liu, H. Zheng, H. Xu, L. Zhang, X. Xu, S. Xu and X. Pan, *Nano Energy*, 2020, **73**, 104753.

117 P. Chen, Y. Bai, S. Wang, M. Lyu, J. H. Yun and L. Wang, *Adv. Funct. Mater.*, 2018, **28**, 1706923.

118 C. Long, K. Huang, J. Chang, C. Zuo, Y. Gao, X. Luo, B. Liu, H. Xie, Z. Chen, J. He, H. Huang, Y. Gao, L. Ding and J. Yang, *Small*, 2021, **17**, 2102368.

119 N. H. Hemasiri, S. Kazim and S. Ahmad, *Nano Energy*, 2020, **77**, 105292.

120 M.-H. Li, T.-G. Sun, J.-Y. Shao, Y.-D. Wang, J.-S. Hu and Y.-W. Zhong, *Nano Energy*, 2021, **79**, 105462.

121 S. Akin, Y. Altintas, E. Mutlugun and S. Sonmezoglu, *Nano Energy*, 2019, **60**, 557–566.

122 X. Zheng, J. Troughton, N. Gasparini, Y. Lin, M. Wei, Y. Hou, J. Liu, K. Song, Z. Chen, C. Yang, B. Turedi, A. Y. Alsalloum, J. Pan, J. Chen, A. A. Zhumekenov, T. D. Anthopoulos, Y. Han, D. Baran, O. F. Mohammed, E. H. Sargent and O. M. Bakr, *Joule*, 2019, **3**, 1963–1976.

123 X. D. Zhu, X. J. Ma, Y. K. Wang, Y. Li, C. H. Gao, Z. K. Wang, Z. Q. Jiang and L. S. Liao, *Adv. Funct. Mater.*, 2019, **29**, 1807094.

124 Z. Hawash, L. K. Ono and Y. Qi, *Adv. Mater. Interfaces*, 2018, **5**, 1700623.

125 F. Cheng, R. He, S. Nie, C. Zhang, J. Yin, J. Li, N. Zheng and B. Wu, *J. Am. Chem. Soc.*, 2021, **143**, 5855–5866.

126 X. Zhu, B. Cheng, X. Li, J. Zhang and L. Zhang, *Appl. Surf. Sci.*, 2019, **487**, 32–40.

127 I. Ka, I. M. Asuo, R. Nechache and F. Rosei, *Chem. Eng. J.*, 2021, **423**, 130334.

128 G. A. Sepalage, S. Meyer, A. R. Pascoe, A. D. Scully, U. Bach, Y.-B. Cheng and L. Spiccia, *Nano Energy*, 2017, **32**, 310–319.

129 I. S. Yang, S. Lee, J. Choi, M. T. Jung, J. Kim and W. I. Lee, *J. Mater. Chem. A*, 2019, **7**, 6028–6037.

130 R. Wang, R. Nakar, Y. Jiang, N. Berton, S. Wu, Q. Wang, J.-M. Liu, G. Zhou, K. Kempa, B. Schmaltz and J. Gao, *J. Mater. Chem. A*, 2020, **8**, 16527–16533.

131 A. Krishna, H. Zhang, Z. Zhou, T. Gallet, M. Dankl, O. Ouellette, F. T. Eickemeyer, F. Fu, S. Sanchez, M. Mensi, S. M. Zakeeruddin, U. Rothlisberger, G. N. Manjunatha Reddy, A. Redinger, M. Gratzel and A. Hagfeldt, *Energy Environ. Sci.*, 2021, **14**, 5552–5562.

132 R. Zhao, L. Xie, R. Zhuang, T. Wu, R. Zhao, L. Wang, L. Sun and Y. Hua, *ACS Energy Lett.*, 2021, **6**, 4209–4219.

133 K. Ma, H. R. Atapattu, Q. Zhao, Y. Gao, B. P. Finkenauer, K. Wang, K. Chen, S. M. Park, A. H. Coffey, C. Zhu, L. Huang, K. R. Graham, J. Mei and L. Dou, *Adv. Mater.*, 2021, **33**, 2100791.

134 S. Wang, Y. Zhu, C. Wang and R. Ma, *J. Mater. Chem. A*, 2019, **7**, 11867–11876.

135 M. Salado, M. Andresini, P. Huang, M. T. Khan, F. Ciriaco, S. Kazim and S. Ahmad, *Adv. Funct. Mater.*, 2020, **30**, 1910561.

136 L. Liang, H. Luo, J. Hu, H. Li and P. Gao, *Adv. Energy Mater.*, 2020, **10**, 2000197.

137 F. Zhang, H. Lu, B. W. Larson, C. Xiao, S. P. Dunfield, O. G. Reid, X. Chen, M. Yang, J. J. Berry, M. C. Beard and K. Zhu, *Chem*, 2021, **7**, 774–785.

138 M. Hou, Y. Wang, X. Yang, M. Han, H. Ren, Y. Li, Q. Huang, Y. Ding, Y. Zhao, X. Zhang and G. Hou, *Nano Energy*, 2022, **94**, 2270009.

139 R. Li, P. Wang, B. Chen, X. Cui, Y. Ding, Y. Li, D. Zhang, Y. Zhao and X. Zhang, *ACS Energy Lett.*, 2019, **5**, 79–86.

140 P. Boonmongkolras, S. D. H. Naqvi, D. Kim, S. R. Pae, M. K. Kim, S. Ahn and B. Shin, *Sol. RRL*, 2021, 2000793.

This journal is © The Royal Society of Chemistry 2022

J. Mater. Chem. C, 2022, **10**, 13611–13645 | **13643**

141 M. A. Mahmud, T. Duong, Y. Yin, H. T. Pham, D. Walter, J. Peng, Y. Wu, L. Li, H. Shen, N. Wu, N. Mozaffari, G. Andersson, K. R. Catchpole, K. J. Weber and T. P. White, *Adv. Funct. Mater.*, 2019, **30**, 1907962.

142 X. Chen, W. Xu, N. Ding, Y. Ji, G. Pan, J. Zhu, D. Zhou, Y. Wu, C. Chen and H. Song, *Adv. Funct. Mater.*, 2020, **30**, 2003295.

143 X. Chen, W. Xu, Z. Shi, G. Pan, J. Zhu, J. Hu, X. Li, C. Shan and H. Song, *Nano Energy*, 2021, **80**, 105564.

144 R. Chen, B. Long, S. Wang, Y. Liu, J. Bai, S. Huang, H. Li and X. Chen, *ACS Appl. Mater. Interfaces*, 2021, **13**, 24747–24755.

145 L. Liu, D. Liu, R. Sun, D. Zhou, Y. Wu, X. Zhuang, S. Liu, W. Bi, N. Wang, L. Zi, B. Zhang, Z. Shi and H. Song, *Sol. RRL*, 2021, **5**, 2000652.

146 Y. Chen, X. Zuo, Y. He, F. Qian, S. Zuo, Y. Zhang, L. Liang, Z. Chen, K. Zhao, Z. Liu, J. Gou and S. F. Liu, *Adv. Sci.*, 2021, **8**, 2001466.

147 S. Zouhair, S. M. Yoo, D. Bogachuk, J. P. Herterich, J. Lim, H. Kanda, B. Son, H. J. Yun, U. Würfel, A. Chahboun, M. K. Nazeeruddin, A. Hinsch, L. Wagner and H. Kim, *Adv. Energy Mater.*, 2022, **12**, 2200837.

148 Z. Wu, Z. Liu, Z. Hu, Z. Hawash, L. Qiu, Y. Jiang, L. K. Ono and Y. Qi, *Adv. Mater.*, 2019, **31**, 1804284.

149 J. Werner, G. Dubuis, A. Walter, P. Löper, S. Moon, S. Nicolay, M. Masis, S. Wolf, B. Niesen and C. Ballif, *Sol. Energy Mater. Sol. Cells*, 2015, **141**, 407–413.

150 D. Akin Kara, K. Kara, G. Oylumluoglu, M. Z. Yigit, M. Can, J. J. Kim, E. K. Burnett, D. L. Gonzalez Arellano, S. Buyukcelebi, F. Ozel, O. Usluer, A. L. Briseno and M. Kus, *ACS Appl. Mater. Interfaces*, 2018, **10**, 30000–30007.

151 J. Huang, K.-X. Wang, J.-J. Chang, Y.-Y. Jiang, Q.-S. Xiao and Y. Li, *J. Mater. Chem. A*, 2017, **5**, 13817–13822.

152 F. Wu, K. Yan, H. Wu, B. Niu, Z. Liu, Y. Li, L. Zuo and H. Chen, *J. Mater. Chem. A*, 2021, **9**, 14920–14927.

153 X. Zhou, M. Hu, C. Liu, L. Zhang, X. Zhong, X. Li, Y. Tian, C. Cheng and B. Xu, *Nano Energy*, 2019, **63**, 103866.

154 K. Jiang, F. Wu, G. Zhang, P. C. Y. Chow, C. Ma, S. Li, K. S. Wong, L. Zhu and H. Yan, *J. Mater. Chem. A*, 2019, **7**, 21662–21667.

155 T. Liu, Y. Jiang, M. Qin, J. Liu, L. Sun, F. Qin, L. Hu, S. Xiong, X. Jiang, F. Jiang, P. Peng, S. Jin, X. Lu and Y. Zhou, *Nat. Commun.*, 2019, **10**, 878.

156 Y.-C. Chin, M. Daboczi, C. Henderson, J. Luke and J.-S. Kim, *ACS Energy Lett.*, 2022, **7**, 560–568.

157 N. J. Jeon, J. H. Noh, Y. C. Kim, W. S. Yang, S. Ryu and S. I. Seok, *Nat. Mater.*, 2014, **13**, 897–903.

158 D. Głowienka, D. Zhang, F. Di Giacomo, M. Najafi, S. Veenstra, J. Szmytkowski and Y. Galagan, *Nano Energy*, 2020, **67**, 104186.

159 M. Wang, H. Wang, W. Li, X. Hu, K. Sun and Z. Zang, *J. Mater. Chem. A*, 2019, **7**, 26421–26428.

160 H. Liu, H.-R. Liu, F. Yang, J.-E. Yang, J. Song, M. Li, Z. Li, W. C. Tsoi, M. Chinweokwu Eze, Z.-Y. Liu, H. Ma, M. Gao and Z.-K. Wang, *J. Power Sources*, 2020, **448**, 227420.

161 Q. Zhou, J. Qiu, Y. Wang, M. Yu, J. Liu and X. Zhang, *ACS Energy Lett.*, 2021, 1596–1606.

162 X. Xu, X. Ji, R. Chen, F. Ye, S. Liu, S. Zhang, W. Chen, Y. Wu and W. H. Zhu, *Adv. Funct. Mater.*, 2022, **32**, 2109968.

163 J. Y. Jeng, K. C. Chen, T. Y. Chiang, P. Y. Lin, T. D. Tsai, Y. C. Chang, T. F. Guo, P. Chen, T. C. Wen and Y. J. Hsu, *Adv. Mater.*, 2014, **26**, 4107–4113.

164 A. S. Subbiah, A. Halder, S. Ghosh, N. Mahuli, G. Hodes and S. K. Sarkar, *J. Phys. Chem. Lett.*, 2014, **5**, 1748–1753.

165 C. X. Guo, K. Sun, J. Ouyang and X. Lu, *Chem. Mater.*, 2015, **27**, 5813–5819.

166 W. Chen, Y. Zhou, G. Chen, Y. Wu, B. Tu, F. Z. Liu, L. Huang, A. M. C. Ng, A. B. Djurišić and Z. He, *Adv. Energy Mater.*, 2019, **9**, 1803872.

167 X. Liu, H. W. Qiao, M. Chen, B. Ge, S. Yang, Y. Hou and H. G. Yang, *Mater. Chem. Front.*, 2021, **5**, 3614–3620.

168 B. Zhang, J. Su, X. Guo, L. Zhou, Z. Lin, L. Feng, J. Zhang, J. Chang and Y. Hao, *Adv. Sci.*, 2020, **7**, 1903044.

169 S. Zhumagali, F. H. Isikgor, P. Maity, J. Yin, E. Ugur, M. De Bastiani, A. S. Subbiah, A. J. Mirabelli, R. Azmi, G. T. Harrison, J. Troughton, E. Aydin, J. Liu, T. Allen, A. U. Rehman, D. Baran, O. F. Mohammed and S. De Wolf, *Adv. Energy Mater.*, 2021, **11**, 2101662.

170 J. Zhang, J. Long, Z. Huang, J. Yang, X. Li, R. Dai, W. Sheng, L. Tan and Y. Chen, *Chem. Eng. J.*, 2021, **426**, 131357.

171 A. Sadhu, M. Rai, T. Salim, X. Jin, J. M. R. Tan, S. W. Leow, M. G. Ahmed, S. Magdassi, S. G. Mhaisalkar and L. H. Wong, *Adv. Funct. Mater.*, 2021, **31**, 2103807.

172 J. Y. Jeng, Y. F. Chiang, M. H. Lee, S. R. Peng, T. F. Guo, P. Chen and T. C. Wen, *Adv. Mater.*, 2013, **25**, 3727–3732.

173 J. You, Z. Hong, Y. M. Yang, Q. Chen, M. Cai, T. B. Song, C. C. Chen, S. Lu, Y. Liu, H. Zhou and Y. Yang, *ACS Nano*, 2014, **8**, 1674–1680.

174 W. Chen, B. Han, Q. Hu, M. Gu, Y. Zhu, W. Yang, Y. Zhou, D. Luo, F.-Z. Liu, R. Cheng, R. Zhu, S.-P. Feng, A. B. Djurišić, T. P. Russell and Z. He, *Sci. Bull.*, 2021, **66**, 991–1002.

175 P. Patil, D. S. Mann, U. T. Nakate, Y.-B. Hahn, S.-N. Kwon and S.-I. Na, *Chem. Eng. J.*, 2020, **397**, 125504.

176 S. Wang, H. Chen, J. Zhang, G. Xu, W. Chen, R. Xue, M. Zhang, Y. Li and Y. Li, *Adv. Mater.*, 2019, **31**, 1903691.

177 H. Wang, F. Yang, N. Li, J. Song, J. Qu, S. Hayase and W.-Y. Wong, *Chem. Eng. J.*, 2020, **392**, 123677.

178 W. Yang, R. Su, D. Luo, Q. Hu, F. Zhang, Z. Xu, Z. Wang, J. Tang, Z. Lv, X. Yang, Y. Tu, W. Zhang, H. Zhong, Q. Gong, T. P. Russell and R. Zhu, *Nano Energy*, 2020, **67**, 104189.

179 R. Ma, Z. Ren, C. Li, Y. Wang, Z. Huang, Y. Zhao, T. Yang, Y. Liang, X. W. Sun and W. C. H. Choy, *Small*, 2020, **16**, 2002628.

180 J. Zhuang, P. Mao, Y. Luan, X. Yi, Z. Tu, Y. Zhang, Y. Yi, Y. Wei, N. Chen, T. Lin, F. Wang, C. Li and J. Wang, *ACS Energy Lett.*, 2019, **4**, 2913–2921.

181 Q. Yang, X. Liu, S. Yu, Z. Feng, L. Liang, W. Qin, Y. Wang, X. Hu, S. Chen, Z. Feng, G. Hou, K. Wu, X. Guo and C. Li, *Energy Environ. Sci.*, 2021, **14**, 6536–6545.

182 B. Li, Y. Xiang, K. D. G. I. Jayawardena, D. Luo, Z. Wang, X. Yang, J. F. Watts, S. Hinder, M. T. Sajjad, T. Webb,

13644 | *J. Mater. Chem. C*, 2022, **10**, 13611–13645

This journal is © The Royal Society of Chemistry 2022

H. Luo, I. Marko, H. Li, S. A. J. Thomson, R. Zhu, G. Shao, S. J. Sweeney, S. R. P. Silva and W. Zhang, *Nano Energy*, 2020, **78**, 105249.

183 Z. W. Gao, Y. Wang, D. Ouyang, H. Liu, Z. Huang, J. Kim and W. C. H. Choy, *Small Methods*, 2020, **4**, 2000478.

184 M. Degani, Q. An, M. A. Siguan, Y. J. Hofstetter, C. Cho, F. Paulus, G. Grancini and Y. Vaynzof, *Sci. Adv.*, 2021, **7**, eabj7930.

185 H. Wang, J. Song, J. Qu, J. Lian, P. C. Qian and W. Y. Wong, *J. Mater. Chem. A*, 2020, **8**, 18117–18124.

186 G. Wang, K. Zhang, Z. Wang, J. Wang, R. Xu, L. Li, X. Xu, Y. Li, S. Xiao, S. Zheng, X. Li and S. Yang, *Nano Energy*, 2021, **89**, 106374.

187 J. Wang, J. Li, Y. Zhou, C. Yu, Y. Hua, Y. Yu, R. Li, X. Lin, R. Chen, H. Wu, H. Xia and H. L. Wang, *J. Am. Chem. Soc.*, 2021, **143**, 7759–7768.

188 X. Li, S. Fu, W. Zhang, S. Ke, W. Song and J. Fang, *Sci. Adv.*, 2020, **6**, eabd1580.

189 Z. Ying, X. Yang, J. Zheng, Y. Zhu, J. Xiu, W. Chen, C. Shou, J. Sheng, Y. Zeng, B. Yan, H. Pan, J. Ye and Z. He, *J. Mater. Chem. A*, 2021, **9**, 12009–12018.

This journal is © The Royal Society of Chemistry 2022

J. Mater. Chem. C, 2022, **10**, 13611–13645 | **13645**